Characterization of Bismuth Ferrite $BiFeO_3$ and Barium Titanate $BaTiO_3$ Films

by

Jiri Vojtech Kabelac

B.S., University of Illinois at Chicago, 1999

M.S., University of Vermont, 2002

THESIS

Submitted as partial fulfillment of the requirements

for the Degree of Doctor of Philosophy in Materials Engineering

in the Graduate College of the

University of Illinois at Chicago, 2011

Defense Committee:

Michael McNallan, Chair and Advisor
Didem Ozevin
Michael Stroscio, Department of Electrical Engineering
Andreas Schroeder, Department of Physics
Farhad Ansari

TABLE OF CONTENTS

LIST OF TABLES

LIST OF FIGURES

LIST OF FIGURES (continued)

LIST OF ABBREVIATIONS

a, b, c – lattice parameters of crystal

d - thickness [Å]

h, k, l – Miller indices

k – relative permittivity

n – index of refraction

n_o – ordinary index of refraction

n_e – extraordinary index of reflection

q – elementary charge ($1.602 * 10^{-19}$ C)

r – specific resistance [Ω]

r_p – amplitude of parallel polarized light

r_s – amplitude of orthogonal polarized light

t – time [s]

x – path difference [rad]

B – magnetic field [G, T]

C – capacitance [F]

G – conductance [S]

H – enthalpy [kJ $mole^{-1}$]

H_c – coercivity [Oe]

I – current [A]

M_r – remanence [emu cm^{-3}]

P – pressure [atm, torr]

P_r – remnant polarization [C cm^{-3}]

LIST OF ABBREVIATIONS (continued)

R – resistivity [Ω]

T_C – Currie temperature [K, °C]

T_N – Néel temperature [K, °C]

V – voltage [V]

α, β, γ – lattice angles

γ – angle with the plane of incidence

λ – wavelength [nm, Å]

Δ – phase shift [rad]

ϕ_1 – angle of refraction of film

ϕ_s – angle of refraction of substrate

μ – mobility [$cm^2 V^{-1} s^{-1}$]

Ψ – azimuth [rad]

ρ – resistance [Ω cm]

θ – angle of incidence of X-ray [deg]

θ_i – angle of incidence of light [deg]

χ – degree of ellipticity [rad]

ω – angle between X-ray path and sample [deg]

I. ABSTRACT

The subject of this thesis is to examine properties of Bismuth Ferrite $BiFeO_3$ (BFO) and Barium Titanate $BaTiO_3$ (BTO) on different substrates, namely $SrTiO_3$ (STO) and Si(001). Unfortunately, due to technical difficulties after certain time period, only a deposition on $SrTiO_3$ was achieved. Both $BiFeO_3$ and $BaTiO_3$ are deposited in molecular beam epitaxy chamber (MBE). Characterization of the films consists of X-ray scans, Rutherford Backscattering, measuring an index of refraction and thickness by an optical method, and electronic measurements as capacitance and relative permittivity. Due to incompatibility of the deposited chromium with the perovskite films, the relative permittivity is in single digits and the other electronics measurements are not performed. The films are grown with different thickness and processing parameters as effusion and substrate temperatures.

It is found that if the ratio of metals is kept close enough to 1.0, the BFO film grows epitaxially for a range of growth rates, from 0.371 to 4.644 Å min^{-1}, despite of the amount of oxygen. The lattice parameter in <001> direction is bigger than 4.02 Å but except in one experiment. The optical methods reveal that there is a tendency the more epitaxial film, the higher the index of refraction and the smaller difference of the index of refraction measured by the polarizing spectrometer and by the Fresnel scan, which is almost always smaller. The index varies from 1.934 to 3.162. Another interesting fact is that the 2theta-omega scan should be done twice, with the sample rotating by 90°, to see whether the scan consist of the same number of peaks. The difference is probably because the film is not close enough to cubic and the X-ray scan is a 3-D problem.

The BTO films are more consistent than BFO films. When it is possible to determine the chemical composition via RBS, then the film is either epitaxial or twinning. The lattice parameter is smaller than for bulk but almost identical to the lattice parameter of the STO substrate. The index of refraction is smaller than for bulk and without the imaginary part.

II. INTRODUCTION

Ceramics with perovskite crystal structure are interesting and useful for their unique properties. They have a very wide range of properties including superconductivity, piezoelectricity, ferroelectricity, colossal magnetoresistance, and magnetostriction [1], and that is why they are used in CMOS devices or optical devices. As well they can be used as chemical sensors, i.e. $Ba_3Ca_{1.18}Nb_{1.82}O_{9-\delta}$ (BCN18) is oxygen ion conductor in dry air but proton conductor in H_2O containing atmosphere at a temperature 700 °C, [2]. They can be used both as single property materials, i.e. in pyroelectronics, or as multiferoic materials, i.e. a coupling as nondestructive examination of one property as a function of the other. Also since they are thermodynamically stable at higher temperatures, it is possible to use them as catalysts in hot gas exhaust systems or as a fuel cell medium.

The most intriguing material properties are produced by coupling of two or more phenomena. This means that one property depends on another and vice versa. In varistors, such as STO, resistivity depends on electrical field, in relaxors as $Pb_xLa_{1-x}ZrO_3$ (x = 0.25) ferroelectricity depends on electrical field, in BFO, piezoelectricity depends on magnetization, Fig. 1 [3].

Perovskites are characterized by structure, which depends on an number of elements involved and their valence, Fig. 2 [1]. The chemical composition is $A_nB_mO_k$, where oxygen is always 2-, and the elements represented by A and B are selected to keep the compound neutrally charged, i.e. $A^{3-}B^{3-}O_3^{2-}$ or $A^{2-}B^{4-}O_3^{2-}$. The chemical composition is not limited to three elements, i.e. a superconductor $HgBa_2Ca_2Cu_3O_{8+x}$. If the perovskite $A_nB_mO_3$ satisfy a tolerance factor t, $0.75 < t < 1.0$

$$t = (r_A + r_O) / [2^{0.5} * (r_B + r_O)] \qquad (1)$$

where r_A, r_B, r_O = radius of elements A, B, and oxygen, then the perovskite is cubic. If it does not, then it is distorted at room temperature as orthorhombic, rhombohedral, tetragonal, monoclinic, or triclinic crystals but it holds cubic structure at higher temperatures.

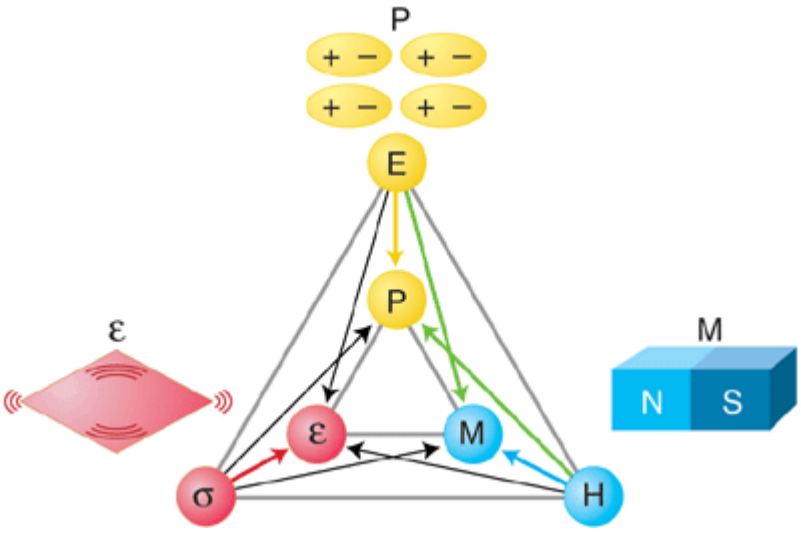

Fig. 1

Schematics of the control of polarization P, magnetization M, and stress σ by electrical field E, magnetic field H, and strain ε, [2].

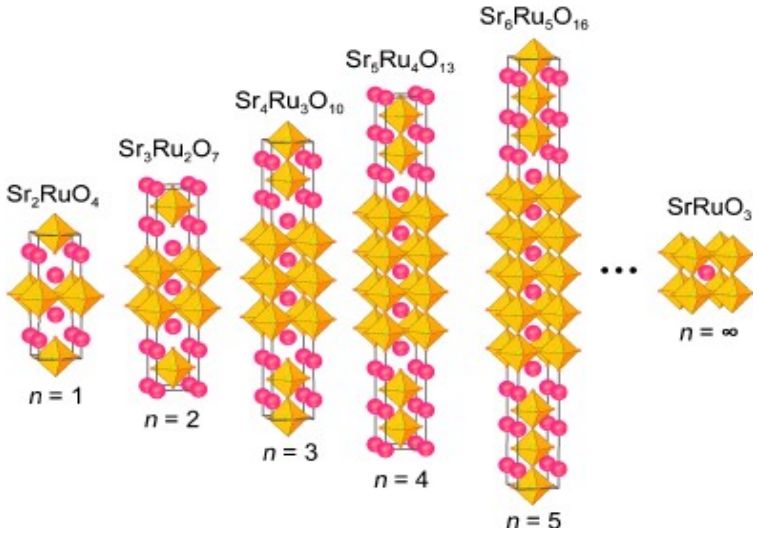

Fig. 2

The compounds follow a series $Sr_{n+1}Ru_nO_{n+1}$. Ru^{4+} lies in the center of the oxygen coordinate octahedra [1].

The high mobility of ions in perovskite is the only negative characteristic and only in the types of CMOS technology where the leakage current is above the limit 10^{-3} A cm^{-2}. It can be eliminated growing the film too high thickness but this may require a high operation voltage in devices. On the other hand, perovskites can have relative permittivity *k* around 100 or more and with suitable technology it can produce *k* above 800 [4].

III. MOLECULAR BEAM EPITAXY

Molecular beam epitaxy (MBE) is one of the techniques used to grow epitaxial films. The epitaxial films are single crystal. This means that the film and substrate have the same structural orientation, i.e. the 2theta – omega scan reveals the family of directions <001> and no other. The epitaxial film is desired if the amount of dangling bonds must be restricted and one needs to grow another epitaxial layer. The chamber must be under ultra high vacuum (UHV) to satisfy a condition that the mean free path, λ is larger than the dimensions of the chamber [5]. This corresponds to a total operating pressure below 10^{-5} torr. The pressure in the MBE chamber during the operation time should be in 10^{-9} to 10^{-11} torr range. The deposited materials are in crucibles and in separate effusion cells that can be closed or opened with a shutter. The materials must be of very high purity and they are heated in crucibles to sublime. The sublimed element is emitted from the crucible as beam, which is defined by the dimensions of the crucible, vapor pressure, and the amount of the element in the crucible as well.
The MBE chamber consists of the growth chamber, effusion cells, plasma source, substrate table, and sensors to measure operational data, Fig. 3. The substrate table can be rotated, tilted or heated.
The deposition procedure begins with increasing temperature in the effusion cells to heat material up to the working temperatures. At the same time, the substrate on a holder is loaded via a loading and buffer chamber (Fig. 4) to the growth chamber, where it is heated to the desired temperature. The plasma is turned on manually. The energy of the plasma keeps the elements in the ionized state and does not allow them to react until they reach the surface of the substrate. When everything is set up, the proper deposition can begin by following a preset program. After the deposition is finished, the program can cool off effusion materials and the substrate but the plasma must be turned off manually. The substrate with a deposited film is unloaded after reaching room temperature. General instructions for the procedure are in Appendix A.

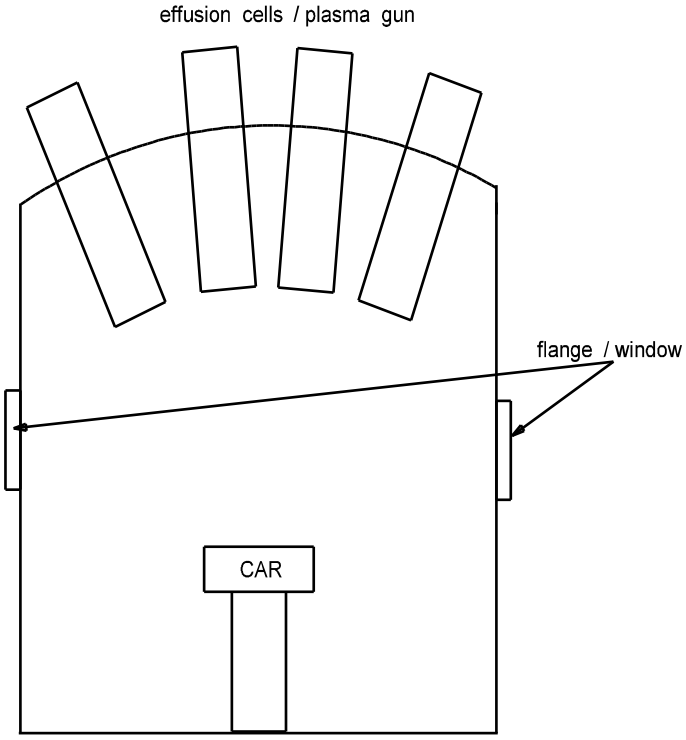

Fig. 3

Schematics of the growth chamber, vertical cut [6].

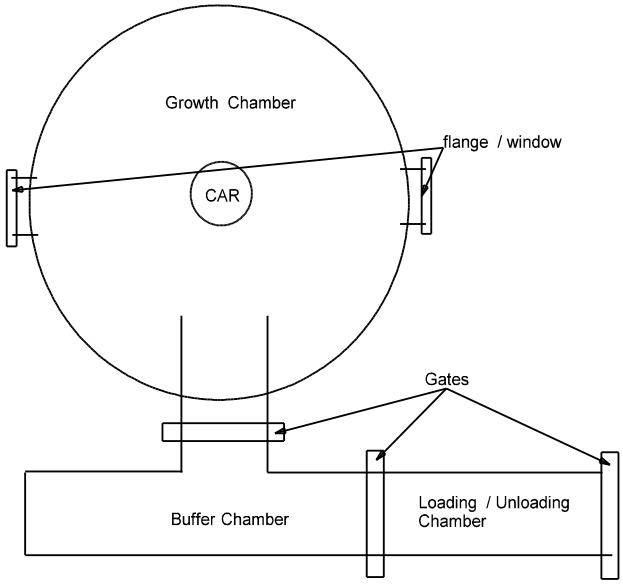

Fig. 4

Schematics of the MBE system, [7].

IV. MATERIALS USED

The deposited films are $BiFeO_3$ (BFO) and $BaTiO_3$ (BTO). As a substrate $SrTiO_3$ (STO) is used and Si(001) was planned. Unfortunately, circumstances did not allow growth on Si.

A. Bismuth Ferrite - $BiFeO_3$

BFO is a rhombohedrally distorted pseudo-cubic perovskite-like structure. The units cell has parameters a =3.96 Å and $\alpha = 89° 29'$, Fig. 5 [8]. BFO is an interesting material for ferroelectric thin films and devices, mainly due to the coexistence of ferroelectric and magnetic orders. Yun *et al.* [9] report a remnant polarization $2P_r = 136$ C / cm^2, remanence $2M_r = 6.0$ emu / cm^3, and coercivity $2H_c =$ 200 Oe for thin films with a thickness = 350 nm. BFO has a high Curie temperature $T_C = \sim 1100$ K and Neel temperature $T_N = \sim 673$ K [10]. Other electrical properties have been measured as well such as tangent loss, relative dielectric constant (up to $k = 1450$, optical band gap ($E_g \approx 2.5$ eV), current leakage, i.e. as in [10, 11, 12]. Its electrical conductivity is around 10^{-4} S cm^{-1} for DC current at room temperature, carrier mobility is still not know yet as well thermal conductivity, so far no one has reported any such measurements both for a bulk or thin films , and index of refraction varies from 1.51 for a porous film grown by the sol – gel method [13] to 2.95 for films grown by pulsed laser and MBE on STO(111) [14]. The values may be of the same order as for other perovskites. i.e. the thermal conductivity of STO is 9.1 W * m^{-1} * K^{-2} doped with 8.4 * 10^{20} cm^{-3} of La and 9.6 W * m^{-1} * K^{-2} doped with 3.3 * 10^{20} cm^{-3} Nb, carrier mobility is 9.2 cm^2 * V^{-1} * s^{-1} for La and 6.0 cm^2 * V^{-1} * s^{-1} for Nb, and conductivity is 1000 S * cm^{-1} for La and 353 S * cm^{-1} for Nb at the room temperature but every parameter decreases with higher temperature [15]. The mean index of refraction can be computed from the Gladstone-Dale relationship and it is $n_{BFO} = 2.62$, but BFO is not optically uni-axial and its

birefringence is $n = n_o - n_e = 0.34$ according to [16]. According to Blaauw *et al.* [8], no phase changes are detected but Krainik *et al.* [17] find structural transitions by measuring the relative thermal expansion but do not say which of them are related to the phase transition.

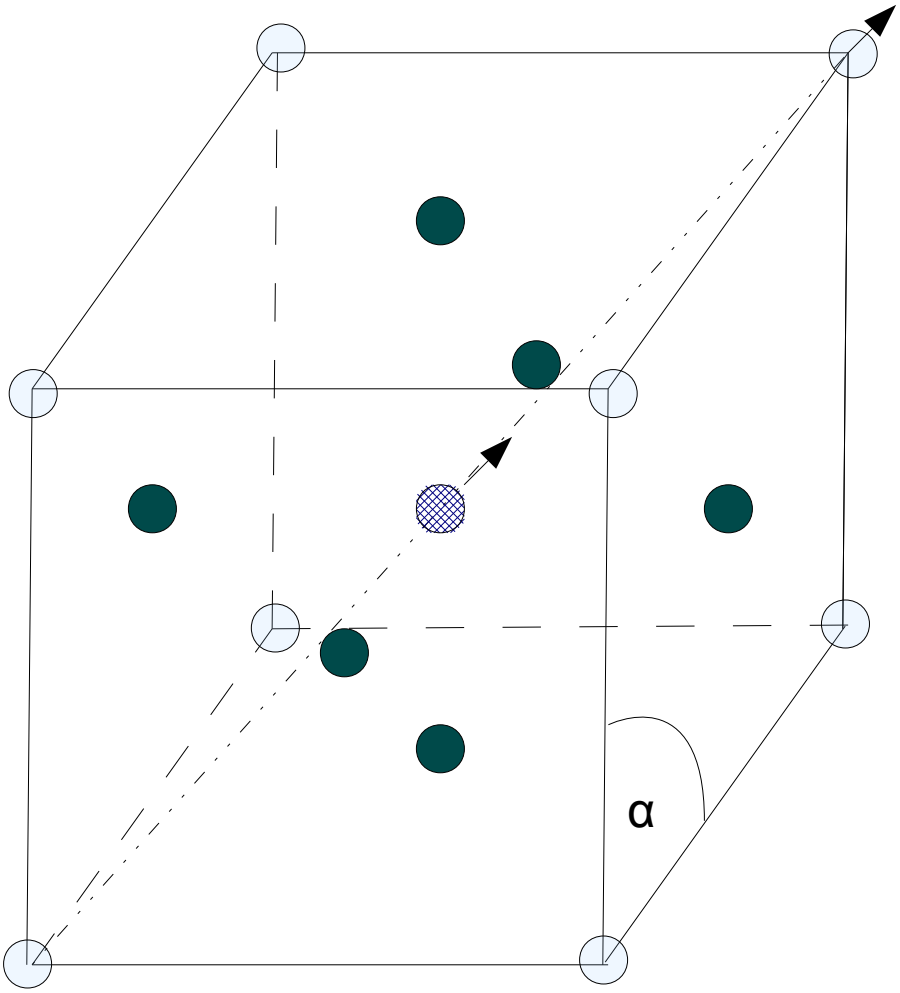

Fig. 5

The ideal (cubic) monomolecular perovskite structure. The arrows indicate the direction [111] of the Fe and Bi ion displacements. Circle with grids – Fe, empty circles – Bi, full circles – oxygen. For BFO: α = 89° 28′, a = 3.96 Å.

B. Barium Titanate – $BaTiO_3$

BTO is the most studied ferroelectric material from any point of view [18]. It goes through four phase

changes. Up to 183 K, it has rhombohedral structure with parameters a = b = c = 4.00 Å and α = β = γ = 89.84º. From 183 K to 278 K, it has orthorhombic structure, a = b = 4.02 Å, c = 3.98 Å, and γ = 89.92º. Between 278 and 393 K, it maintains tetragonal structure, a = b = 3.99 Å, c = 4.03 Å. Above 393 K, BTO is cubic with a = 4.012 Å. Its electric resistivity about 10^2 Ω cm for thin films can be deduced from [19] and the resistivity for the bulk is 10^{11} Ω cm, relative permittivity k = 1350, index of refraction 2.362 + i1.14 for wavelength 625 nm [20], and thermal conductivity 2.2 – 3.2 W K^{-1} m^{-1} [21].

C. Silicon dioxide - SiO_2

The task of SiO_2 is to create the oxide layer to induce a stress relaxation between BFO and a substrate. The mechanism of growing BFO on Si(001) is described by the Fig. 6. The SiO_2 itself is amorphous. It is not used in a combination with perovskites but it is employed extensively in CMOS technology. It is an insulator with a resistivity of 10^{14} - 10^{16} ohm * cm, relative permittivity k = 3.9, index of refraction 1.46 for wavelength 630 nm, and thermal conductivity 1.38 W K^{-1} m^{-1} [22]. It can be grown thermally on a Si substrate. In state-of-the-art technology, SiO_2 is not suitable for thicknesses of 20 Å or less, since the leakage current rises to 1 – 10 A cm^{-2}, which is well over the limit 10^{-3} A cm^{-2}.

D. Silicon - Si

Silicon has a diamond cubic structure, Fig.7, with a lattice parameter a = 5.4309 Å. It is a semiconductor and its conductivity depends highly on dopants, as shown in Fig.8. Silicon is the most used element in the electronics industry because of its versatility and compatibility with SiO_2. Another reason for the widespread use of Si is its low cost. It is possible to make relatively cheap devices and Si is compatible with other elements and compounds. Index of refraction of Si is 3.4255 for wavelength 630 nm, its relative permittivity is 11.8, and its thermal conductivity is 124 W K^{-1} m^{-1} [22].

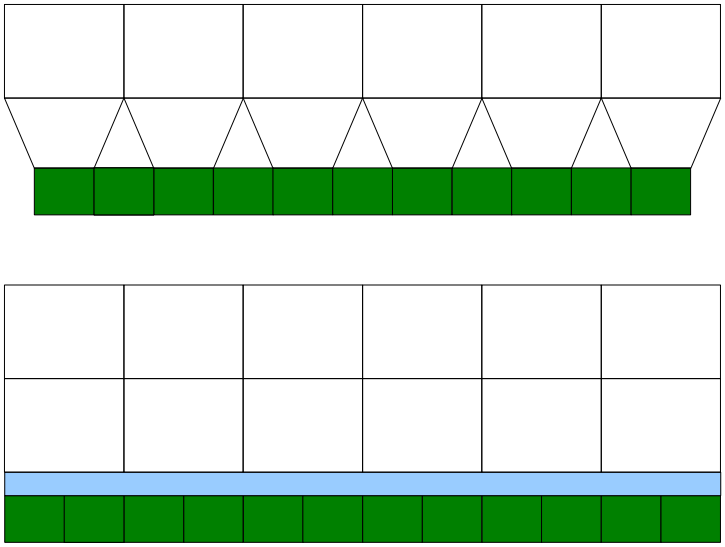

Fig. 6

Mechanism of releasing stress between Si substrate and film.

In the part above, the deposited material is stressed. In the lower part, it is relaxed thanks to SiO_2.

Full small squares – Si, Grid large squares – film, layer between Si and film – SiO_2. Not to scale.

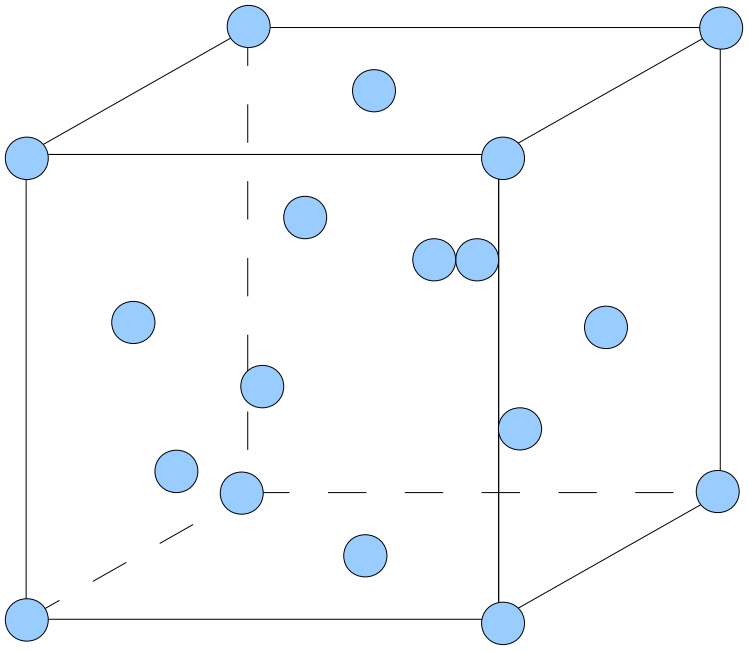

Fig. 7

Diamond structure of silicon.

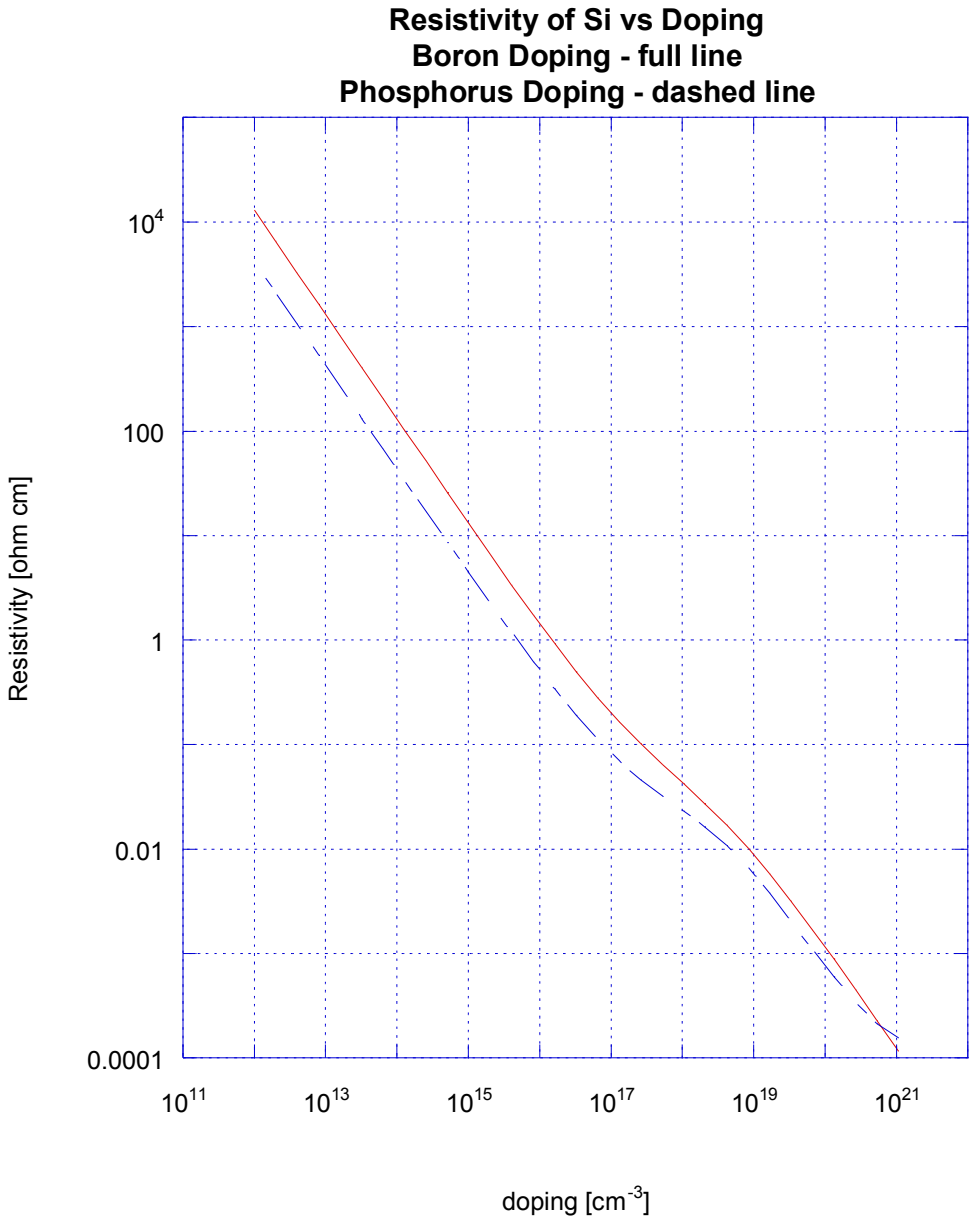

Fig. 8

Plot Resistivity vs. Doping

Full line – Boron, Dashed line – Phosphorus.

E. Strontium Titanate – $SrTiO_3$

STO is used as a substrate because of a lattice match with BFO and thermal stability to avoid any kind reaction or diffusion. It is cubic at room temperature with a lattice parameter a = 3.905 Å. Its crystallographic structure, very similar that of BFO, is with Ti in the center. This perovskite has an electrical resistivity around 10^{13} ohm * cm [23], a relative permittivity k = 300, an index of refraction of 2.39 for wavelength 630 nm [24], and thermal conductivity of 3.7 – 5.8 W K^{-1} m^{-1} [23].

V. GROWTH ASSUMPTIONS

The growing assumptions are different for STO and Si(001). STO is inert to BFO, both have the same crystal structure, and the lattice mismatch in the <001> direction is only 1.4%. On the other hand, it would be difficult and much more expensive to make devices on STO. BFO has a mismatch with Si(001) equal to 37% and one can not eliminate undesirable reactions on the BFO – substrate film either with silicon on silicon dioxide. However, in the direction <111> of BFO, the mismatch is only 3.12%:

$$\text{mismatch} = (3.96 * 2^{0.5} - 5.43095) / 5.43095 = 3.12\% \qquad (1)$$

The mismatch geometry is illustrated in Fig. 9. BFO can also be grown on Si(001) [10]. Wang e*t al.* report [10] that BFO grows in the <001> direction and with no other material except the expected material is detected with pulsed laser deposition. This technique provides a thin film deposition technique where a high power pulsed laser beam is focused at a target in a high vacuum chamber. No one has reported the growth of BFO by MBE. On the other hand, Tisinger *et al.* have managed to grow thin films of STO on Si(001) in <001> directions [25].

As of this article, no one has grown perovskite with the native oxide on. The big unknown is a chemical reaction at the interface of film – Si substrate. But one can suppose that BFO, as a ceramics that has a large decomposition enthalpy, would be the most favorable product and no byproduct is produced by Bi, Fe, and Si.

The deposition is made on STO. It is the task of research to determine details but according to [15], it is possible to grow an epitaxial thin film of Yttria Stabilized Zirconia (YSZ) at the room temperature both on etched and unetched Si(001) and even without a plasma.. It is reasonable to grow BFO on Si(001), since BFO is thermodynamically similar to YSZ.

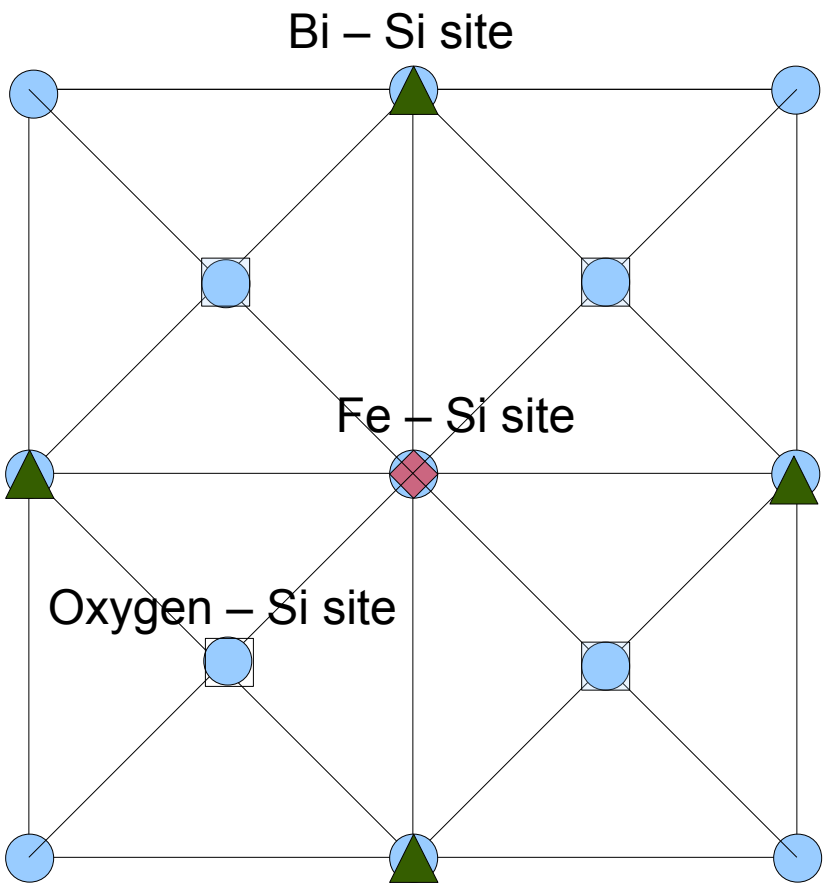

Fig. 9

Geometrical schematics of Silicon – BFO interface.

Dark square – Fe, triangles – Bi, empty squares – oxygen, full circles – Si.

The dissociation enthalpy of YSZ is taken as for pure ZrO_2 and is equal to $\Delta H = -1098.2$ kJ mole^{-1}, which is almost of the same order as for BFO, $\Delta H = -770.6$ kJ mole^{-1}. The dissociation enthalpy of BFO is computed from the equations (2) [26], (3), and (4):

$$\tfrac{1}{2}Bi_2O_3 + \tfrac{1}{2}Fe_2O_3 \rightarrow BiFeO_3,\ \Delta H \approx \Delta G = -70.8 \text{ kJ mole}^{-1} \qquad (2)$$

$$2Bi + 1.5\ O_2 \rightarrow Bi_2O_3,\ \Delta H = -574.3\ kJ\ mole^{-1},\ \Delta G = -493.8\ kJ\ mole^{-1} \quad (3)$$

$$2Fe + 1.5\ O_2 \rightarrow Fe_2O_3,\ \Delta H = -825.5\ kJ\ mole^{-1},\ \Delta G = -743.5\ kJ\ mole^{-1} \quad (4)$$

Since YSZ reacts on Si substrate with SiO_2 either forming silicon monoxide SiO(g) or Si according to reactions (5) and (6):

$$Zr(g) + 2SiO_2 \rightarrow ZrO_2 + 2SiO(g),\ \Delta G = -280.472\ kJ\ mole^{-1} \quad (5)$$

$$Zr(g) + SiO_2 \rightarrow ZrO_2 + Si,\ \Delta G = -639.688\ kJ\ mole^{-1} \quad (6)$$

It can be supposed that BFO would react with the substrate material in a similar manner. All the reactions above are computed for P = 1 atm and at room temperature. The influence of a very low pressure and mainly plasma will shift the reactions to the right.

VI. TESTS TO EXAMINE THE FILMS

The tests are divided into two sections. The first one is a set of non-destructive tests and the other one involves a procedure that alters the film's surface by a deposition of metal. The first section consists of X-ray scans, Rutherford backscattering scan, and examination with a spectrometer. The second section involves measurements of electrical properties, Hall effect tests, and capacitance measurements.

A. X-ray Scans

The X-ray scan consists of 2theta-omega, omega, and phi scans. The 2theta-omega scan is run twice. After the first scan, the sample is rotated by 90° and the second scan is run under the same parameters. The reason is that once before a sample was scanned twice; after the first scan, the sample was accidentally rotated, and the number of peaks of the 2theta-omega scan was changed. The 2theta-omega scan determinates a lattice parameter in out-of-plane direction, but not in-plane lattice dimensions. The omega scan indicates quality by single peak and it is very empirical. One measures the full-width-at-half-maximum (FWHM) and must be compared to another parameter. The phi scan determinates how epitaxial the film is by comparing to the known scan.

In this type of 2theta-omega scan the omega angle is a half of the theta angle, as indicated in Fig. 10. The diffraction obeys according to the Bragg's Law:

$$2 * d * \sin\theta = n * \lambda \qquad (7)$$

$$d = a / (h^2 + k^2 + l^2)^{0.5} \text{ for a cubic system} \qquad (8)$$

where d - distance between two planes of atoms, as in Fig. 11, λ is the wavelength of X-rays in Â, n = 1, 2, 3, …, a is the lattice parameter of cubic crystal in Â, h, k, l are the Miller indices.

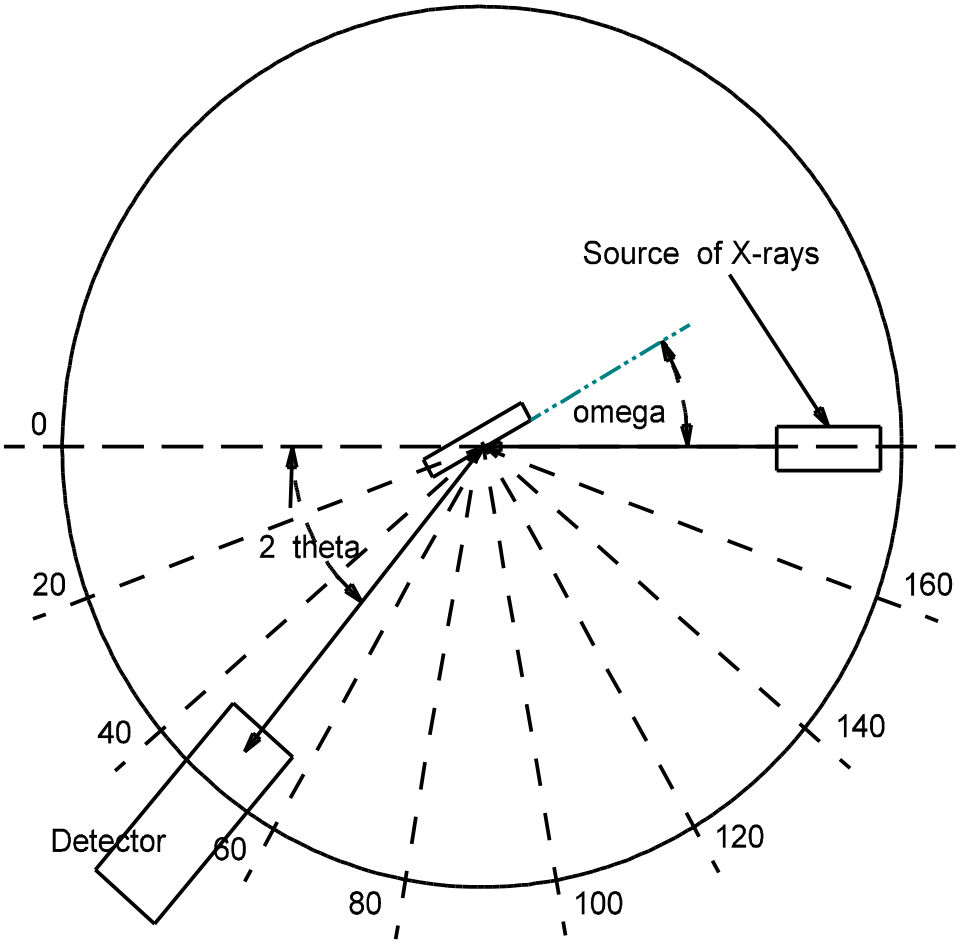

Fig. 10

Schematics of 2theta - omega scan.

The combination of (7) and (8) give an equation to compute the lattice parameter *a*:

$$a = \lambda * (h^2 + k^2 + l^2)^{0.5} / (2 * \sin\theta) \qquad (9)$$

The main purpose of the X-ray scan is to determine lattice parameters, phases, and quality of the film. In the case of epitaxial film, it is possible to determine only a lattice parameter in the c-direction, out of plane.

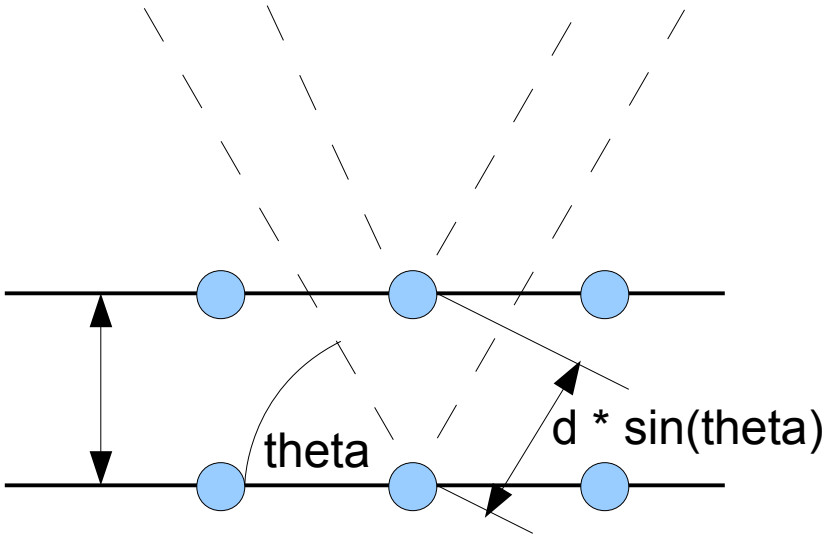

Fig. 11

Schematics illustrating Bragg's Law.

B. Rutherford Backscattering

Rutherford backscattering (RBS) is very useful scanning technique, since one can get information about both chemical composition and thickness at the same time. This scan is very reliable but the data are not very accurate. RBS may be described as an elastic (hard-sphere) collision between a high kineticenergy particle from the incident beam (the projectile) of He ions and a stationary atom located in the sample (the target). Elastic in this context means that no energy is either lost or gained during the collision, so that the energy of reflected beam is related to the mass of the particle that it collided with and, accordingly, the compositional depth profile can be determined from an RBS measurement, as illustrated in Fig. 12. The elements contained in a sample can be determined from the positions of

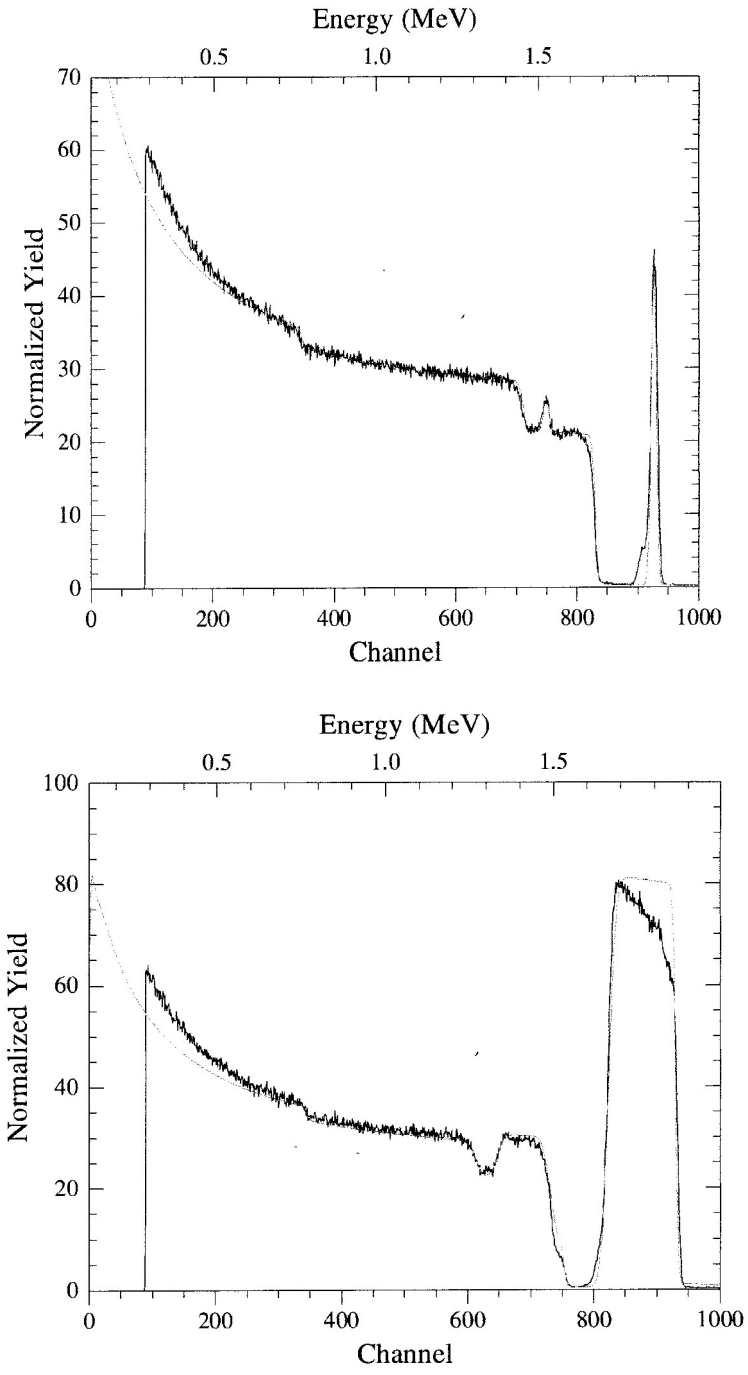

Fig. 12

RBS scan of homogenous epitaxial film (above) and film, which has a roughness (below).

peaks in the energy spectrum. Depth can be determined from the widths and shifted positions of these peaks, and relative concentration from the peak heights. This is especially useful for the analysis of a multilayer sample, for example, or for a sample with a composition which varies more continuously with depth [27].

C. Measurements made with the polarizing spectrometer

The index of refraction and thickness are computed from the optical scan data made with a spectrometer. The algorithm to compute a thickness is taken from [27] and a photo of the actual spectrometer is in Fig. 13. It is the same setup as for an ellipsometer but the difference is in moving parts. The source of light is a diode emitting a red light of wavelength = 635 nm.

The ellipsometer keeps the incident angle of light constant but the analyzer is rotating. The intensity of light is recorded according to the equation

$$I(t) = I_0 * (1 + \alpha * \cos(2 * \omega * t + A_c) + \beta * \sin(2 * \omega * t + A_c)) \qquad (10)$$

where t = time in s, ω = angular speed of analyzer in rad * s^{-1}, A_c, α, β are constants.

In the spectrometer setup, the incident angle is changing, the polarizer is set to give a polarized light with an angle 45° to the sample, and the analyzer is set to allow the light go through either in the orthogonal or parallel direction.

The base of the algorithm is Fresnel's equations. For the substrate with no film, the equations are

$$r_p = \tan(\theta_i - \phi_s) / \tan(\theta_i + \phi_s) \qquad (11a)$$

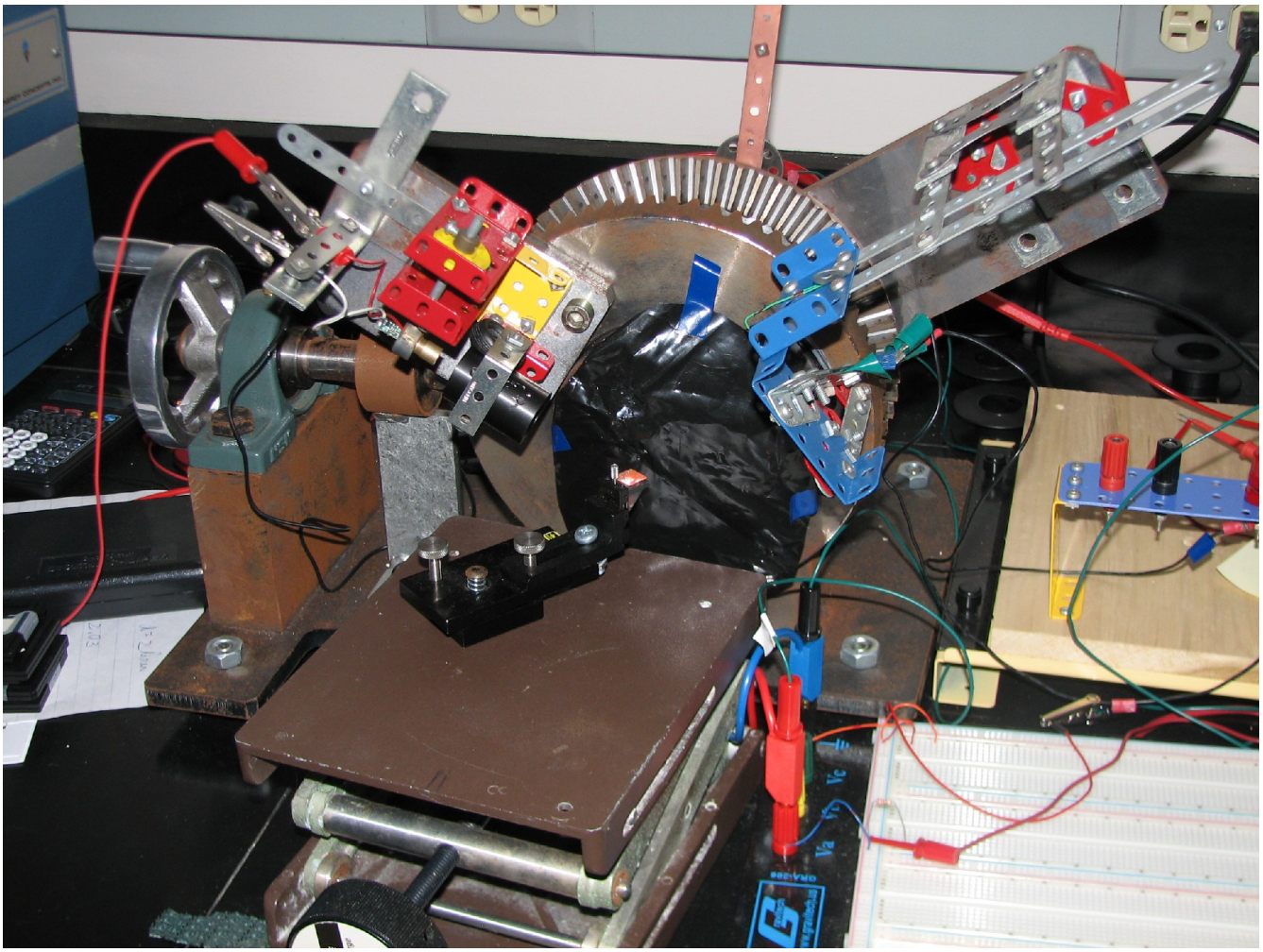

Fig. 13

Polarizing ellipsometer.

$$r_s = - \sin(\theta_i - \phi_s) / \sin(\theta_i + \phi_s) \qquad (11b)$$

where θ is the angle of incidence, ϕ_s is the angle of refraction in the substrate, amplitude reflection coefficient r_p describes the light parallel to the plane of incidence and r_s is orthogonal to the plane of incidence, as in Fig. 14. The equations for the single film and substrate of the polarized light are

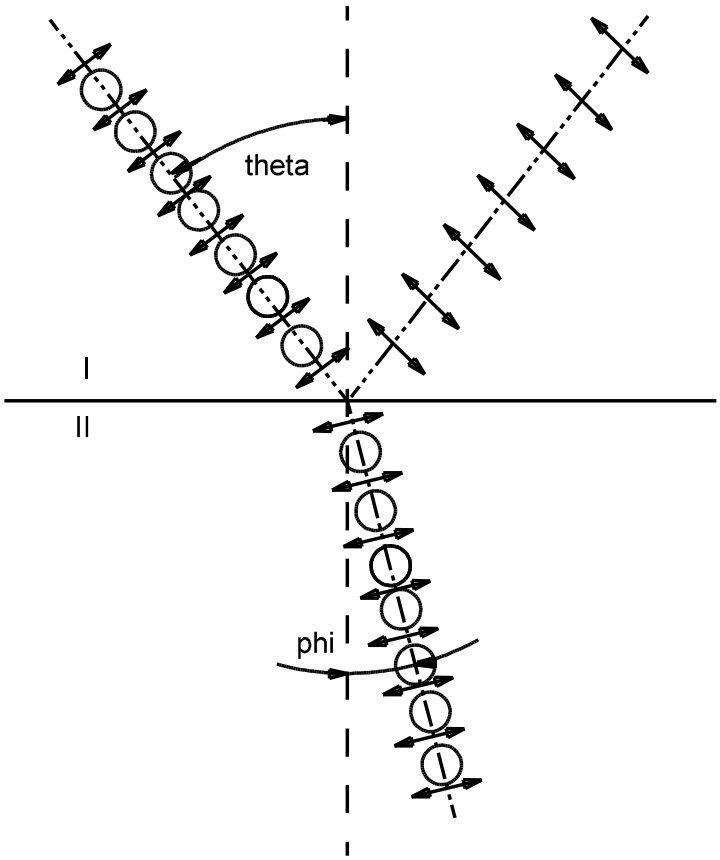

Fig. 14

Diffraction and reflexion on boundaries of media I and II.

Circles – Orthogonal light, Arrows – Parallel light.

theta ≡ θ_i, the incident angle, phi ≡ φ_1, reflection angle in the film

$$r_p*\exp[i*\delta_p] = (r_p' + r_p''*\exp[-i*x]) / (1 + r_p'*r_p''*\exp[-i*x]) \qquad (12a)$$

$$r_s*\exp[i*\delta_s] = (r_s' + r_s''*\exp[-i*x]) / (1 + r_s'*r_s''*\exp[-i*x]) \qquad (12a)$$

where δ_p and δ_s are phase shifts, x is the path difference between boundaries I and II [27], as in Fig. 15:

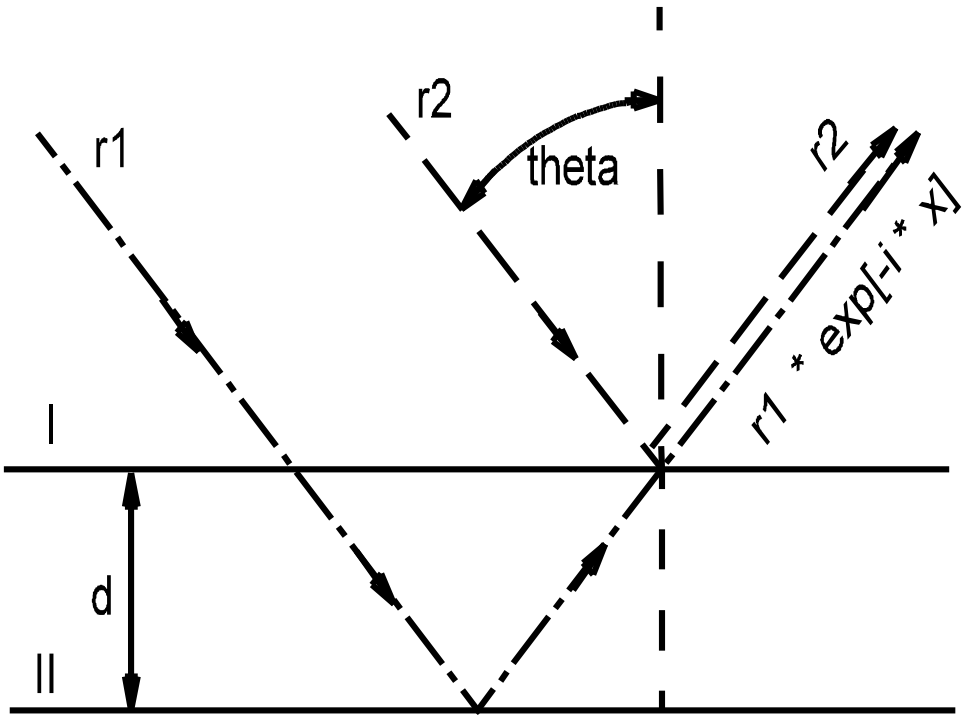

Fig. 15

The reflection of the light on a substrate with a single film.

theta ≡ θ_i, the incident angle.

$$x = 2 * \pi / \lambda * 2 * n_1 * d * \cos[\phi_1] \qquad (13)$$

where λ is wavelength of the incident light, d is thickness of the film, and ϕ_1 is the refraction angle in the film.

The amplitude components r_p', r_p,", r_s", and r_s" are given by the formulas

$$r_p' = \tan(\theta_i - \phi_1) / \tan(\theta_i + \phi_1) \qquad (14a)$$

$$r_p'' = \tan(\phi_1 - \phi_s) / \tan(\phi_1 + \phi_s) \qquad (14b)$$

$$r_s' = - \sin(\theta_i - \phi_1) / \sin(\theta_i + \phi_1) \qquad (14c)$$

$$r_s'' = - \sin(\phi_1 - \phi_s) / \sin(\phi_1 + \phi_s) \qquad (14d)$$

It is necessary to make a note that the refractive index *n* is a real part of a complex index N, N = n+i*k. In practice this means that one will collect data of the absolute amplitude of $\left| r_p \right| = \left| \mathrm{Re}\{r_p\} + \mathrm{Im}\{r_p\} \right|$ or $\left| r_s \right|$; Fig. 16 provides an example for the case of parallel light. The equation is actually

$$r_p * \exp[i*\delta_p] = (r_p' + r_p''*\exp[-i*x]) / (1 + r_p'*r_p''*\exp[-i*x]) \qquad (15)$$

and after multiplying Eqn. 15 by a complex conjugate of the denominator, one separates Eqn. 15 into a real and imaginary parts:

$$\mathrm{Re}\{r_p\} = (r_p' + r_p'' * \cos(x) + r_p'^2 * r_p'' * \cos(x) + r_p' r_p'') / \text{denominator} \qquad (16)$$

$$\mathrm{Im}\{r_p\} = (-r_p'' * \sin(x) + r_p'^2 * r_p''* \sin(x)) / \text{denominator} \qquad (16)$$

where the denominator = $1 + (r_p' * r_p'')^2 + 2 * r_p' * r_p'' * \cos(x)$.

The intensity I of $\left| r_p \right|$ reaches zero at a certain incident angle only if $k = 0$, which is called the Brewster's angle.

The intensity at the Brewster's angle corresponds to the value of the imaginary part of r_p. From the Brewster's angle it is possible to compute the index of refraction according to the equation

$$n_1 / n_0 = \tan(\theta_B) \qquad (17)$$

where n_0 is the refractive index of air (usually taken as 1.0), and θ_B is the Brewster's angle. If the minimum intensity is not equal a zero, then the imaginary part is not a zero as well. If the refractive index is known, then it is possible to determine the thickness of the film by using a quadratic equation to determine the path difference x, Eqn. 13, according to [28]:

$$\cos(x) = (-b + (b^2 - 4 * a * c)^{0.5}) / (2 * a) \qquad (21)$$

where $a = h * h' * (1 - (\tan\Psi)^2)$

$b = f * h' + g' * h - (\tan\Psi)^2 * (f' + g * h')$

$c = f * g' - f' * g * (\tan\Psi)^2$

$f = r_p'^2 + r_p''^2$

$f' = r_s'^2 + r_s''^2$

$g = 1 + r_p'^2 * r_p''^2$

$g' = 1 + r_s'^2 * r_s''^2$

$h = 2 * r_p' * r_p''$

$h' = 2 * r_s' * r_s''$

$\tan\Psi = r_p / r_s$

The solution is unique, since only the positive sign of the square root must be considered [28]. This method consists of two steps. The first one is to determine the index of refraction by the spectrometer scan and then to compute the thickness with a general method from [29], for one must have relatively close approximation of the index of refraction and to determine a quadrant in which the solution is, see the Table I. The equipment consists of spectrometer, multimeter, and power source. The multimeter is

$n_1 < n_2$	cos(x)	quadrant
TRUE	positive	I
TRUE	negative	II
FALSE	positive	III
FALSE	negative	IV

Table I

Determination of quadrant.

Fluke 45, which can measure a voltage and current at the same time. The power source is of a bench type. The variable voltage can go from 0 to 12 V DC. There are two fixed sources as well. One is 5 V DC and the other is 7.5 V AC. The angle is measured at the same time with intensity as electrical values recorded by Fluke software. The intensity is recorded as a current and the angle corresponds to a certain voltage.

The relationship between the voltage and angle was measured before any test was performed. First the lines are separated by 10 cm and are marked on two wooden planks. Then both planks are attached to a ceiling above the spectrometer. A laser module is attached to one of the rotating wheels of the spectrometer. A reference point or angle was determine with a spirit level and transparent plastic. Then voltages and positions of the laser light spot on the plank are recorded. A set of measurements are made and the data shows that the relationship between V vs. Angle is linear, as in Fig. 17. That is why one needs to record only the initial and final angle, which is represented by the first and last voltage, since the initial and final voltage varied little. From the data taken, a plot of I vs. Angle is made, where the current I represents the intensity of polarized refracted light. The minimum is determined from a curve fit of polynomial in the vicinity of the minimum.

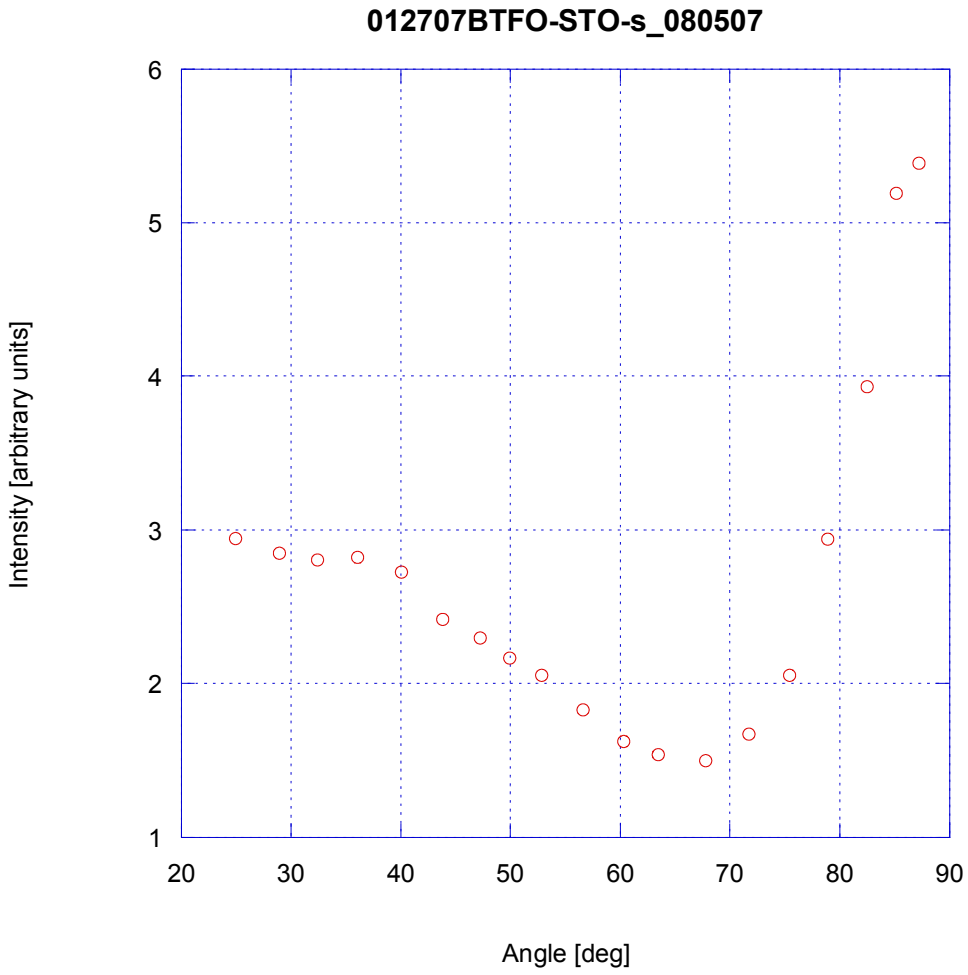

Fig. 16

The scan of Barium Titanate – Bismuth Ferrite Film.

It reveals that the index of refraction is complex.

Three programs are written in FORTRAN95 to solve the equations above. One is used for films thick enough to use the method from [28], the second program is for very thin films, and the third one is when the azimuth angle Ψ is known. The first program is a bisection method to get the thickness, the

other computes a minimum thickness to satisfy a real solution of the quadratic equation, Eqn. 21. The third program computes directly the thickness from the angle Ψ, which is described in following sentences. The intensity is measured as a function of polarization tilt of polarizer, each 10° each corresponds to the a full circle of 360°. The data form an Intensity I vs. Angle plot. The maximum, minimum, and their average are taken along with a corresponding angle to determinate the angle χ as an angle to the plane of incidence and the ellipticity angle γ to solve the Eqn. 22 and 23; this is done since the values of angles Ψ and Δ can not be measured directly [28]:

$$\cos(2 * \Psi) = \cos(2 * \gamma) * \cos(2 * \chi) \qquad (22)$$

$$\tan(\Delta) = \tan(2 * \gamma) / \sin(2 * \chi) \qquad (23)$$

The spectrometer method works as well for films with its index imaginary part not equal a zero, as in Figs. 16 and 18. The procedure is straightforward. First, one makes a Fresnel type scan to get the principal angle of the film; secondly, it is necessary measures the angles χ and γ to compute the angles Ψ and Δ, and computes the thickness and real part of the index of refraction, and then using these values, gets an imaginary part of the index of refraction for the corresponding principal angle. The program to compute the thickness and index of refraction is in Appendix B.

If the principal angle is the same as the Brewster angle, then it is possible to simplify the program. The procedure is straightforward; see Appendix C.

To verify the procedure for how to determine the index of refraction and thickness, the procedure and data from [28] were used. The procedure is described as a general method on p. 147 in [28]. This means one can use data of any angle of incidence to determine the final values, but it is supposed that the index of refraction is approximately known. Vasicek at [28] uses a substrate with the index of

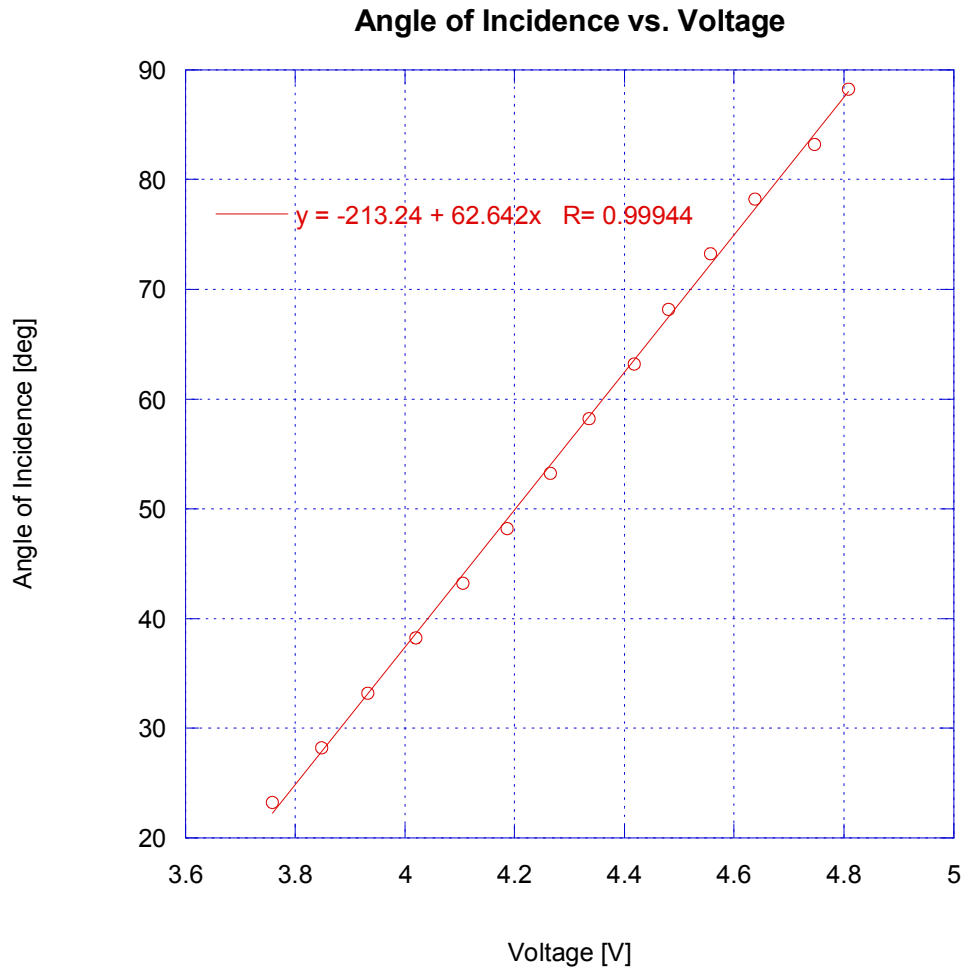

Fig. 17

Plot Angle of Incidence vs. Voltage.

refraction $n_s = 1.5687$ and the index of refraction of the film is around 1.37.

The procedure in [28] is described as follows:

"The mathematical problem of finding the index *n* and the thickness d of the film from Ψ and Δ at

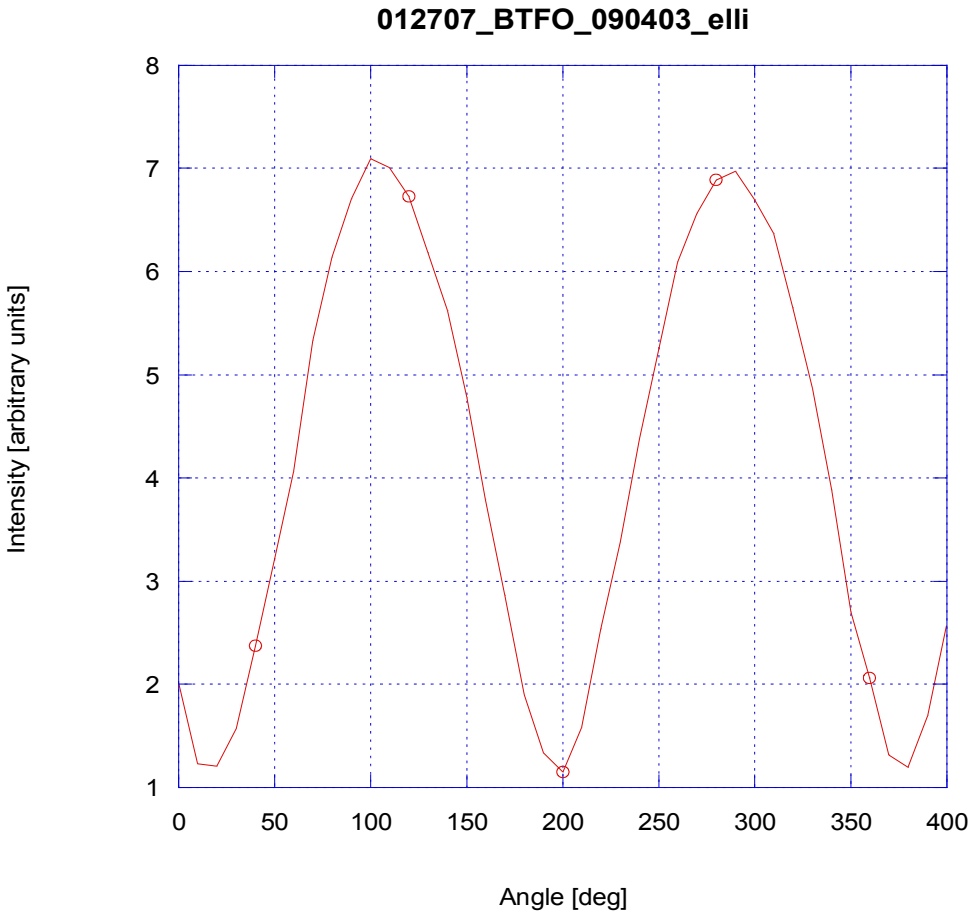

Fig. 18

Ellipsometer – like Scan of Barium Titanate – Bismuth Ferrite Film.

a fixed angle of incidence involves the solution of the two equations, (23) and (24), with respect to *n* and *d*. Unfortunately, it is impossible to give these solutions in explicit form. However, we have succeeded in developing a method, which furnishes the answer by means of graphical interpolation."

$$\tan(\Delta) = (A*B' + A'*B) / (A*A' - B*B') \qquad (24)$$

$$\tan \Psi = [(r_p'^2+r_p''^2+2*r_p'*r_p''\cos(x))*(1+r_s'^2*r_s''^2+2*r_s'*r_s''*\cos(x)) /$$

$$(1+r_p'2*r_p''^2+2*r_s'*r_s''*\cos(x))*(r_s'2+r_s''^2+2*r_s'*r_s''*\cos(x))]^{0.5}, \quad (25)$$

where

$$A = \alpha_1 * \beta_2 + \beta_1 * \beta_2 \quad (26a)$$

$$A' = \alpha_3 * \alpha_4 + \beta_3 * \beta_4 \quad (26b)$$

$$B = \alpha_1 * \beta_2 - \alpha_2 * \beta_1 \quad (26c)$$

$$B' = \alpha_4 * \beta_3 - \alpha_3 * \beta_4 \quad (26d)$$

and

$$\alpha_1 = r_p' + r_p'' * \cos(x) \qquad \beta_1 = r_p'' * \sin(x) \quad (27a)$$

$$\alpha_2 = 1 + r_p' * r_p'' * \cos(x) \qquad \beta_2 = r_p' * r_p'' * \sin(x) \quad (27b)$$

$$\alpha_3 = r_s' + r_s'' * \cos(x) \qquad \beta_3 = r_s'' * \sin(x) \quad (27c)$$

$$\alpha_4 = 1 + r_s' * r_s'' * \cos(x) \qquad \beta_4 = r_s' * r_s'' * \sin(x) \quad (27d)$$

The author chooses initial values of n = 1.350, 1.370, and 1.390. The correct value is expected to be around 1.37. The next step is to compute the optical path difference x for each value of n and for a given value of Ψ. Then the corresponding value of angle Δ is computed with Eqn. (24). From the plot Δ vs. n, the correct value of n is read for the observed angle Δ, [28].

The following step is to compute the path difference x. The mathematical approach is described with the Eqn. 20. It is necessary to note one must decide in which quadrant the solution is. When $n_1 < n_s$, then the solution is either in the quadrant I or II. And if the calculated cos(x) is positive, the x value

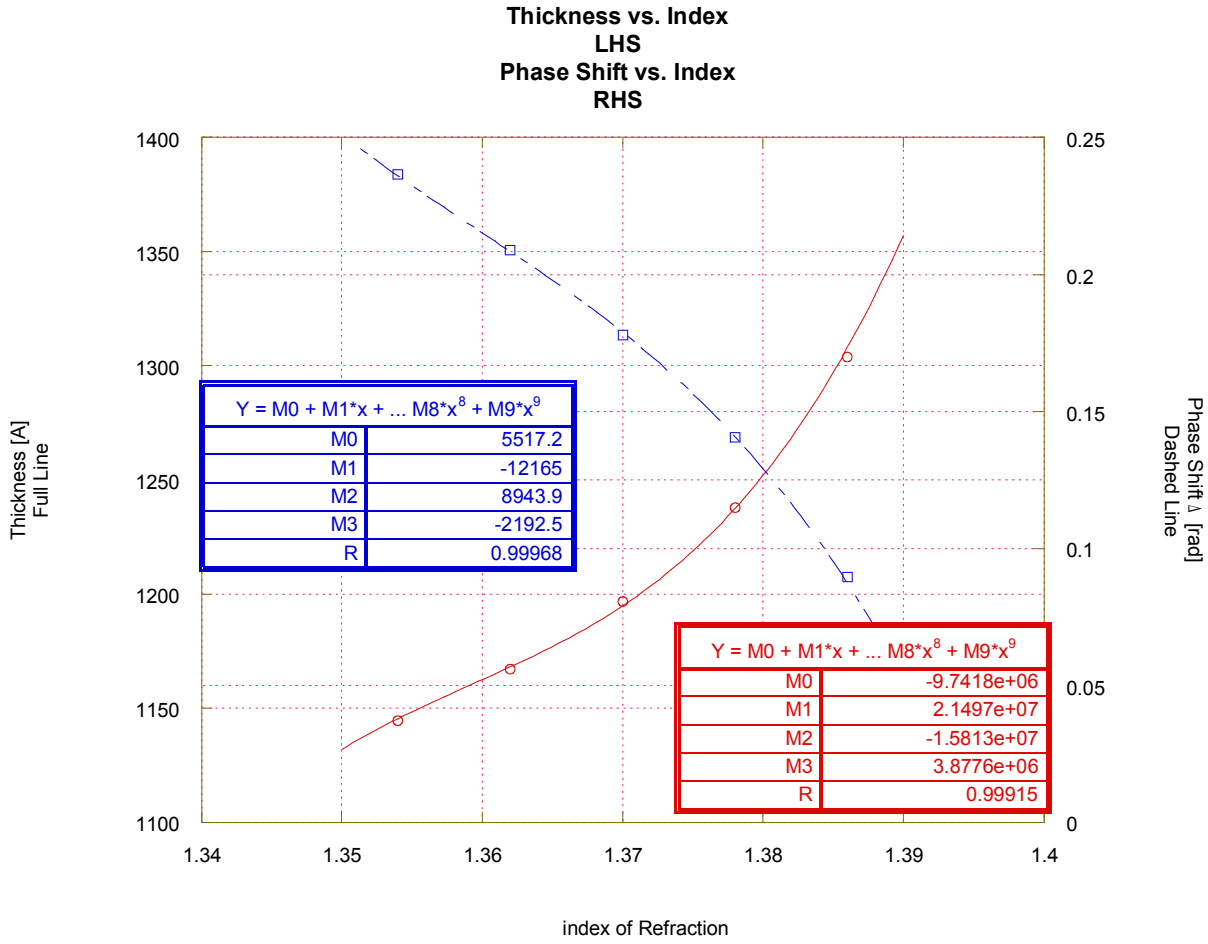

Fig. 19

Double Plot of Thickness vs. Index of Refraction and Phase Shift vs. Index of Refraction. Data taken from [28].

lies in the quadrant I or III; see Table I. The analytical solution and data by Vasicek [28] are in the Fig. 19 and Table II. The author of this paper followed the instructions in [27] using different approach; a numerical method was used instead of a graphical one. The data from the Table II were used and the fact that the angle Δ can be described by two different equations, (24) and (28).

n_1	1.35	1.37	1.39
r_p'	-0.21723	-0.21661	-0.21568
r_s'	-0.47833	-0.48910	-0.49932
r_p''	0.020520	0.019887	0.018909
r_s''	-0.128890	-0.115030	-0.101680
f	0.047603	0.047315	0.046874
g	1.0000199	1.0000186	1.0000166
h	-0.0089146	-0.0086154	-0.0081562
f'	0.245410	0.252450	0.259600
g'	1.003800	1.003170	1.002580
h'	0.123300	0.112520	0.101540
Ψ	29°04'00"	29°04'00"	29°04'00"
tanΨ	0.555830	0.555830	0.555830
a	-0.00075962	-0.00066993	-0.00057234
b	-0.040498	-0.037408	-0.034134
c	-0.028035	-0.030530	-0.033226
cos x	-0.703680	-0.827700	-0.989800
x	134°33'41"	145°51'45"	171°48'30"
sin x	0.712500	0.561190	0.142490
A	-0.232390	-0.233930	-0.235340
A'	-0.375150	-0.377600	-0.378760
B	-0.013931	-0.010637	-0.002569
B'	-0.070820	-0.049110	-0.010876
Δ	14°07.0'	10°01.0'	2°16.0'

Table II

Data Used in [26] to Compute the Index of Refraction and Thickness.

$$\tan\Psi * \cos\Delta = (A*A' - B*B') / (\alpha_2^2+\beta_2^2) / (\alpha_3^2+\beta_3^2) \qquad (28)$$

Saying it in other words, the angle Δ is not independent. For a single film with thickness *d* the index of refraction *n*, and tanΨ, there is a unique value of Δ. The algorithm is rather simple. Two values of refraction are set: One of them is lower than and the other higher than the expected value. Then the average is taken and cos(x) is computed using Eqn. 21. After this the cos(x) is substituted into Eqn. 24. If the value of the angle Δ from the Eqn. 28 was higher than from the Eqn. 24, then the lower value of index remains the same and the new higher value is the first average. This procedure, which is called the bisection method, is to continue until the desired ending.

This procedure could be avoided if the index of refraction were known. One could use the Eqn. 21 directly to solve for cos(x) and then the Eqn. 13 to get the thickness *d*, since all data are available.

The program in Appendix B is used to compute the index *n* and thickness *d* for given data in [28]. The values from [28] and given by the program are in the Table III. The comparison shows a minimal difference.

Source	Index of Refraction	Thicknesses [À]
Vašíček [24]	1.3632	1170
Program, Appendix B	1.3699	1198
Error [%]	0.4910	2.39

Table III

Comparison table of results from [26] and from the program.

D. Hall Effect Test

In order to determine both the mobility and the sheet charge density, n_s, a combination of a resistivity measurement and a Hall measurement is needed. It is performed on a magnet base probe station of my own construction, Fig. 20, and both the resistivity and the Hall voltage are measured with this probe

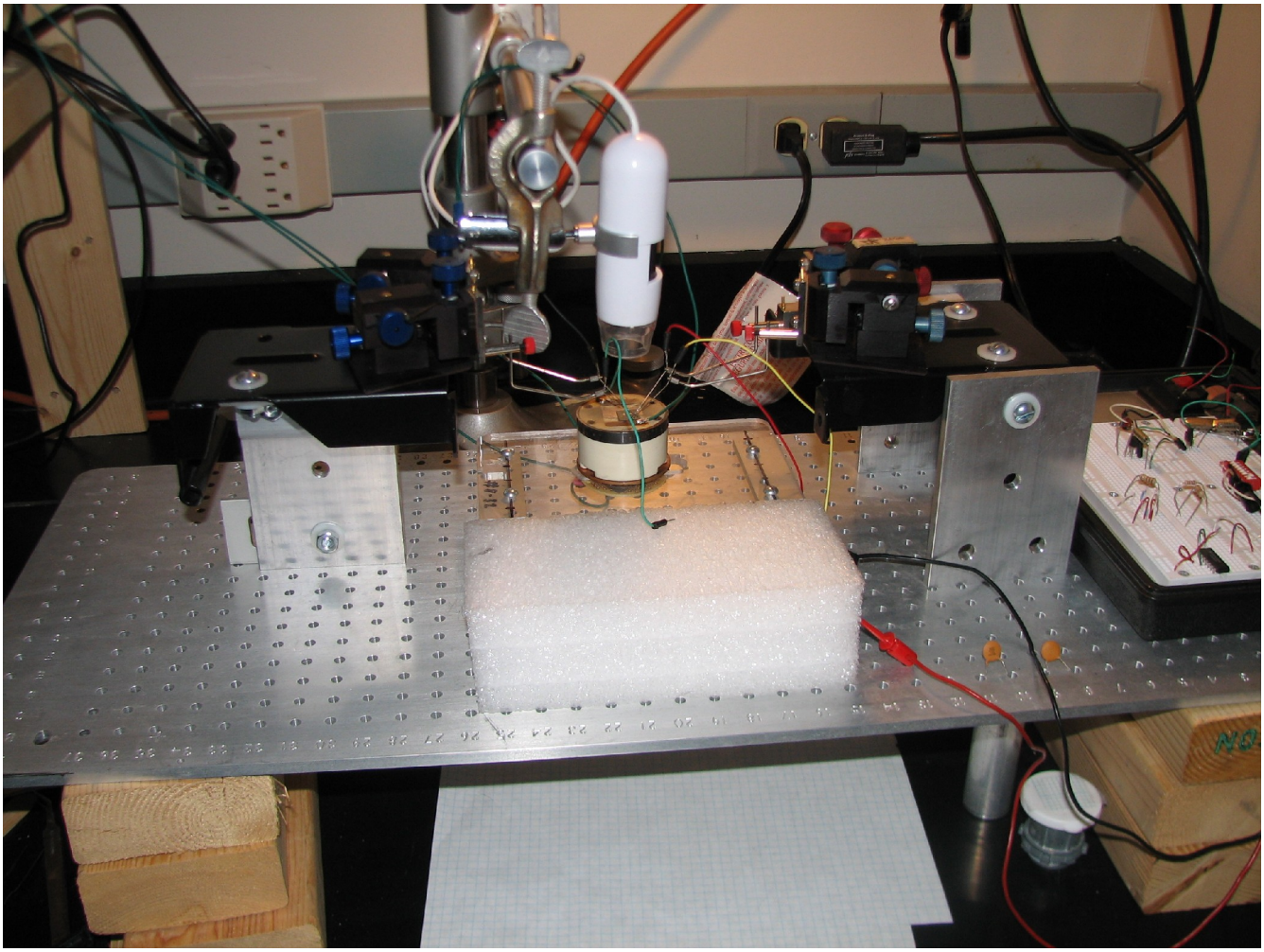

Fig. 20

Photo of the Hall effect probe station.

station. The resistivity is measured with the van der Pauw technique, as illustrated in Fig. 21:

$$R_A = V_{43} / I_{12} \qquad R_B = V_{14} / I_{23} \qquad (29)$$

$$\exp[-\pi * R_A / R_S] + \exp[- \pi * R_B / R_S] = 1.0 \qquad (30)$$

R_S - sheet resistance [ohm]

If the conduction layer thickness is known, then the mobility μ is:

$$\mu = V_H / (R_S * I * B) = 1 / (q * n_s * R_S) \qquad (31)$$

where $n_s = n * d$ - sheet density

I - current [A] = I_{13} or = I_{24}

B - magnetic field [G, T]

q - elementary charge (1.602E-19 C)

V_H - Hall voltage = V_{24} (I_{13}) or = V_{13} (I_{24}), as in Fig. 21.

The measured data also depends on other aspects as ohmic contact quality and size, sample uniformity, accurate thickness determination, thermomagnetic effect due to non uniform temperature distribution, photoconductive and photovoltaic effects which can be minimized by measuring in a dark environment [29].

It is necessary to distinguish between the conductivity mobility μ and Hall mobility μ_H. The relationship is:

$$\mu_H = r * \mu \qquad (32)$$

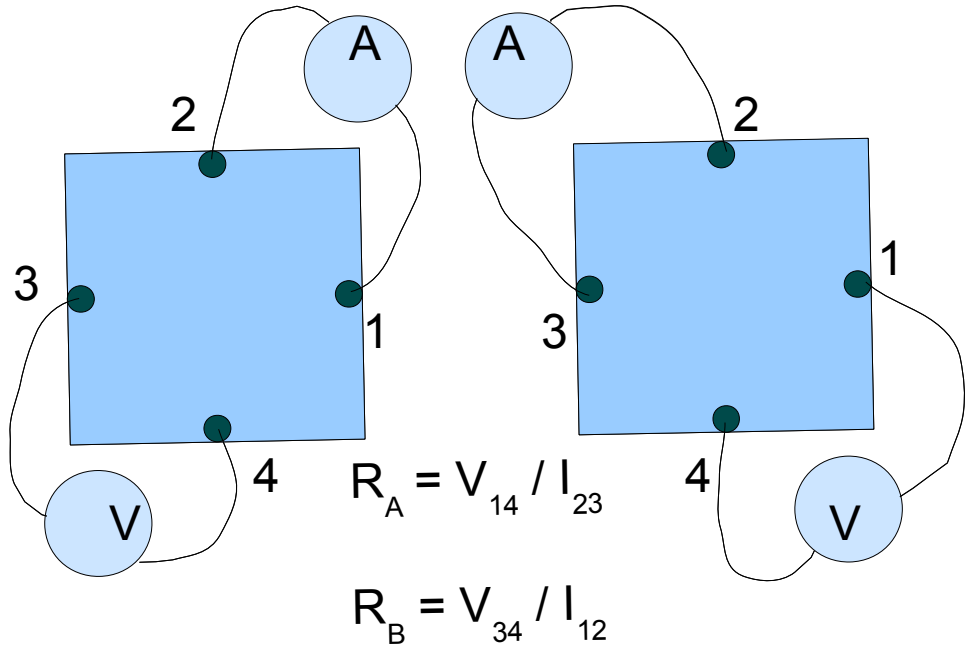

Fig. 21

Schematics of the van der Pauw Technique.

A = ampmeter, V = voltmeter

where $r > 1.0$. The Hall mobility is determined by measuring the van der Pauw resistance with and without a magnetic field. The the Hall mobility is defined as

$$\mu_H = d * \Delta R / B / \rho \qquad (33)$$

where d = thickness [cm]

and

ρ = resistivity [ohm * cm]

E. Current Dependent Capacitance

To measure the capacitance exactly is to use a circuit as in Fig. 22. This method is very simple and one can measure a capacitance under a load as well [30]. The capacitance C is

$$C = I : (\partial V / \partial t) = I * \Delta t / \Delta V \qquad (34)$$

Δt - change of time [s]

ΔV - change of voltage [V]

I - current [A]

If dependence of ΔV vs. Δt is linear, then the device is purely capacitive.

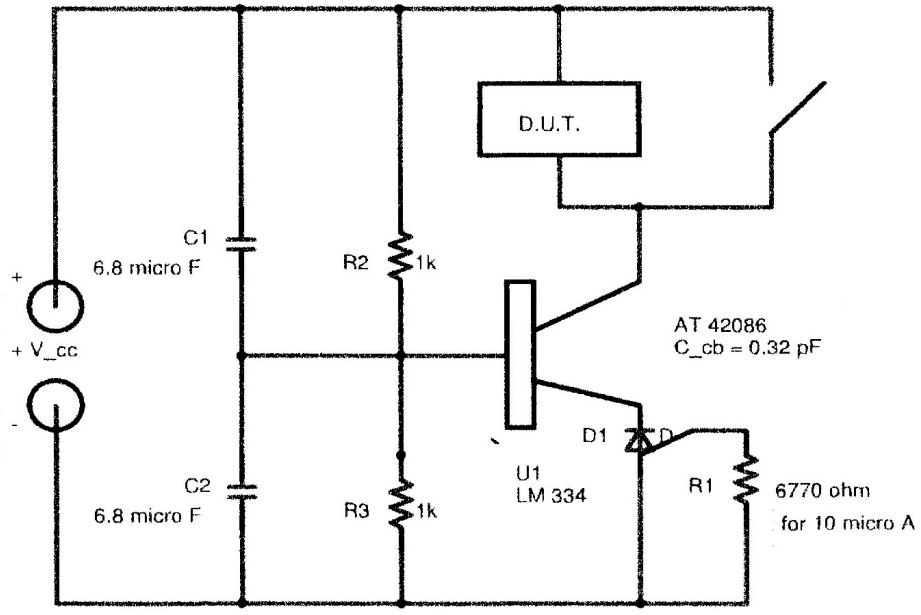

Fig. 22

Circuit to measure Capacitance vs. Voltage.

F. Capacitance vs. Frequency

The last but not least one is the measurement of capacitance vs. frequency [31]. The technique determines the actual capacitance of a film as well the capacitance under a range of frequencies, i.e., due to different mobilities of charge carriers. As well, it deals with a potential error in the series resistance. If the back contact resistance r_s is a problem it may be advantageous to leave the oxide on the back surface and place the wafer on a probe station, thus making a large-area capacitive back

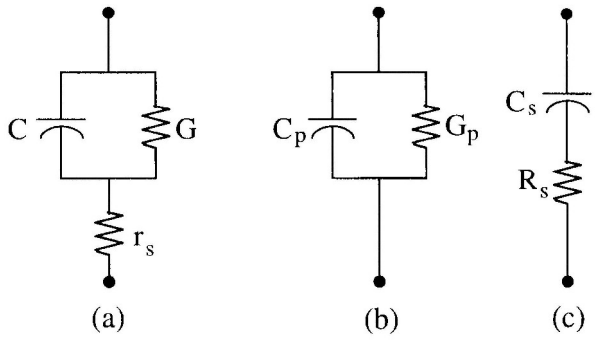

Fig. 23

Circuits to Measure Capacitance.

contact, as illustrated in Figs. 23a and 23b. The contact capacitance C_c is much larger than the device capacitance because its area is usually the area of the entire sample. Such a large capacitance approximates a short circuit. A *p-n* or Schottky diode consists of a junction capacitance C, a junction conductance G, and a series resistance R_s as represented in Fig. 23c.

Capacitance meters assume the device to be represented by either the parallel equivalent circuit Fig. 24a or the series equivalent circuit Fig. 24b. Combining these two circuits into one results in the mathematical description below, which permit C_p, G_p, C_s, and R_s to be written as

$$C_p = C / [(1 + r_s * G)^2 + (\omega * r_s * C)^2] \qquad (35)$$

$$G_p = [G * (1 + r_s * G) + r_s * (\omega * C)^2] / [(1 + r_s * G)^2 + (\omega * r_s * C)^2] \qquad (36)$$

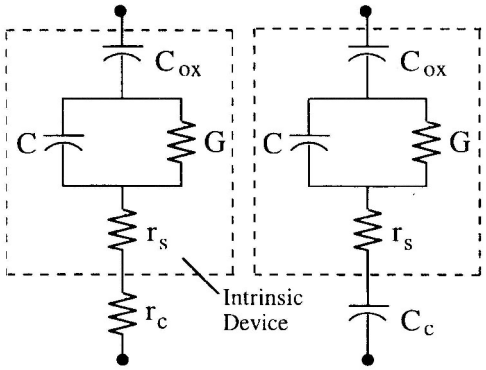

Fig. 24

Equivalent Circuits for Contact Resistance (left) and Contact Capacitance (right).

$$C_s = C * [1 + G / (\omega * C)^2] \qquad (37)$$

$$R_s = r_s + 1 / G / [1 + (\omega * C / G)^2] \qquad (38)$$

The description of variables is in Fig. 23 and 24.

The method of ratios was used to compute the dielectric capacitance. It is supposed that the gate capacitance C and the gate conductance G are constant over the entire range of frequencies. Then two set of data are substituted to the Eqn. 39 and the two compared:

$$\omega * C / G = F / [1 - G_m * r_s * (1 + F^2)] \qquad (39)$$

where $F = \omega * C_m / G_m$

G_m - measured conductance

C_m - measured capacitance

The $(\omega_2 * C / G) / (\omega_1 * C / G)$ is a ratio of the two frequencies that is LHS of the equation and the numbers $(\omega_1 * C_{m1} / G_{m1})$ and $(\omega_2 * C_{m2} / G_{m2})$ are substituted into its RHS. The only unknown is the series resistance r_s. After solving for the r_s, the capacitance is computed by Eqn. 35.

VII. COMPUTING AND EVALUATION PROCEDURES

A. Sample Evaluation of the X-ray Scan

One can determinate from the X-ray scan whether the film is epitaxial or not and compute a lattice parameter in the <001> direction. The film is epitaxial if the peaks of 2theta-omega, omega, and phi scans are smooth and single. If one of the scans is distorted by some way, i.e. there is a double peak or a sub-peak, the film is twinning or even not epitaxial. The scale to determine it is in Fig. 25.

I would like and have to mention about the sample 012907BFO/STO and its 2theta-omega scans. The sample is scanned twice with a rotation of 90°. One of the scan is missing a peak of (001) plane. It could mean that the sample is not pseudo-cubic and the X-ray refraction is not 1-D problem as it is described in text books but 3-D one. It means for BFO samples that the angle α is different than expected. The scans are in Fig. 26.

The lattice parameter is computing according to Eqn. 9 and for all peaks of the X-ray scan. The X-ray wavelength λ = 1.540562 Å. Average of the corresponding peaks was taken but only the data from [001] family. As the sample the data of 122205BFO/STO and are in Table IV.

122205BFO/STO				
2 θ	22.033°	44.773°	69.680°	
plane	001	002	003	Average lattice parameter [Å]
lattice parameter [Å]	4.031	4.045	4.045	4.040
2 θ	31.750°	64.752°	N/A	
plane	011	022	033	Average lattice parameter [Å]
lattice parameter [Å]	3.982	4.069	N/A	4.026

Table IV

Sample computing of the lattice parameter.

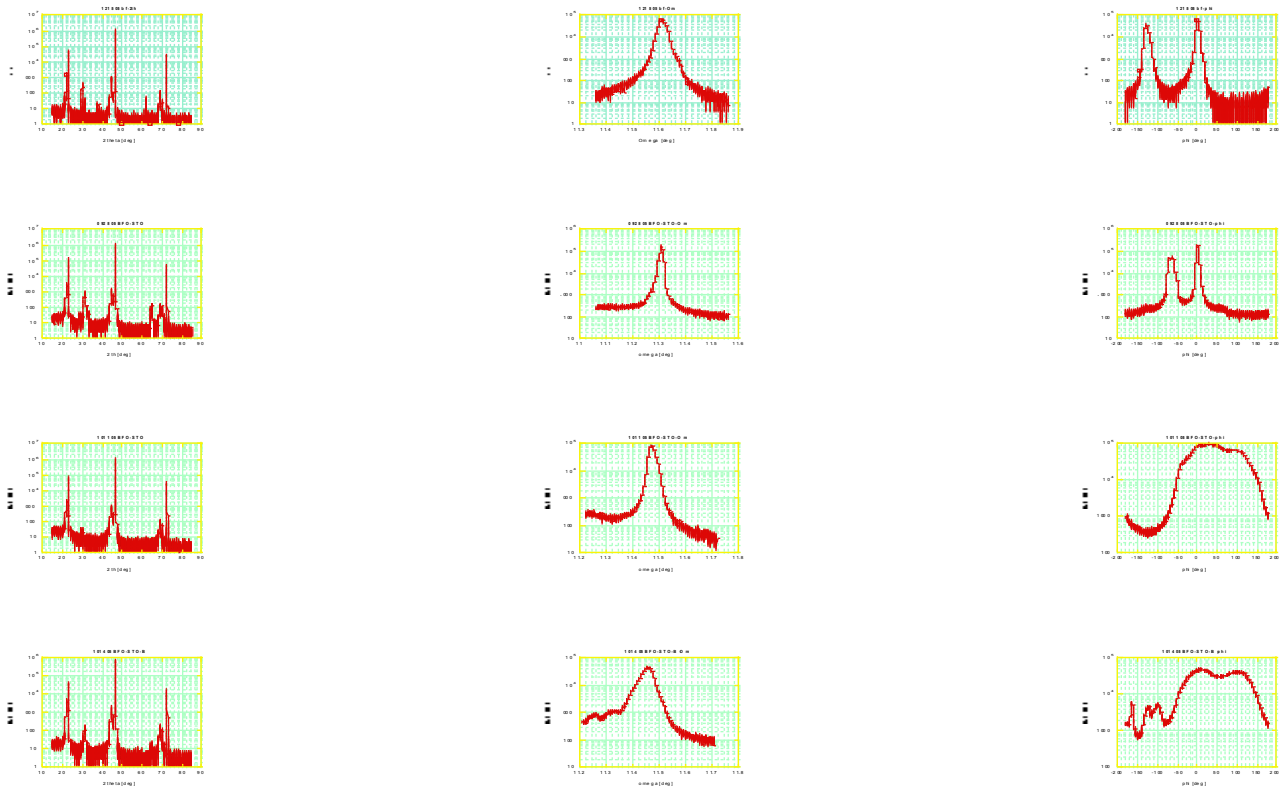

Fig. 25

Scans to determinate the quality of films

Left Column – 2theta-omega scans, Middle – Omega scans, Right – Phi scans

Top Row – Epitaxial Sample of 121505BFO/STO

Second Row – Twinning Sample of 092805BFO/STO

Third and Bottom Row – Not Epitaxial Samples of 101105BFO/STO and 101405BFO/STO_B

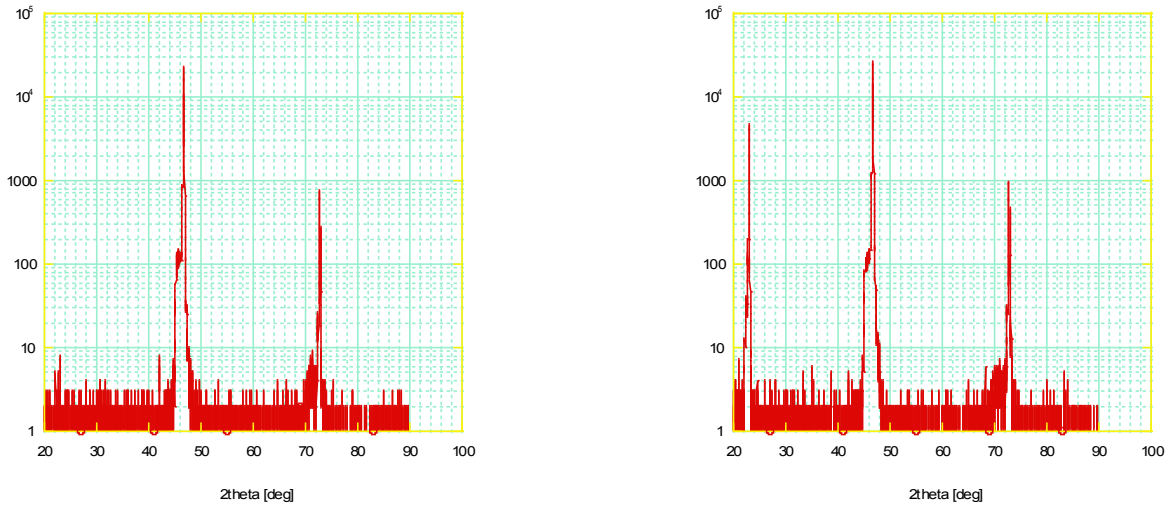

Fig. 26

2theta-omega scans of the sample 012907BFO/STO.

B. Sample Computing of Index of Refraction and Thickness

As the example is taken the 101005BFO/STO sample. The polarizer that receives the reflected light is rotated by 380° - 400° with steps of 10°. The reason why the scan goes over 360° is that one of the minimum may have data only on one side of the peak. Four or three scanned data of minimum or maximum are taken into account. The number depends on whether the region is odd or even symmetrical. The scan data are put to a plot and a polynomial fit is applied in the KaleidaGraph software. From the polynomial fit the angle and intensity of the minimum or maximum is computed. The ellipsometry-like scan is in Fig. 27.

Computing the angle of the plane of incidence γ and ellipsity χ of the polarized light and following computing of the azimuth Ψ and phase shift δ is below:

Minimum I:

$$\text{Intensity } I = -1.3917 * 10^{-5} * z^3 + 0.0015293 * z^2 - 0.03968 * z + 0.34056$$

$$\partial I / \partial z = -4.175 * 10^{-5} * z^2 + 0.0030586 * z - 0.03968 = 0$$

$$z = 16.848°$$

$$I = 0.040$$

Minimum II:

$$I = 1.8333 * 10^{-6} * z^3 - 0.00021 * z^2 - 0.12838 * z + 19.461$$

$$\partial I / \partial z = 5.4999 * 10^{-6} * z^2 - 0.00042 * z - 0.12838 = 0$$

$$z = 195.663° - 180° = 15.663°$$

$$I = 0.035$$

$$\text{Average Minimum} = 0.037$$

Maximum I;

$$I = -0.000645 * z^2 + 0.112735 * z - 4.34$$

$$\partial I / \partial z = -0.00129 * z + 12735 = 0$$

$$z = 98.721° - 90° = 8.721°$$

$$I = 1.946$$

Maximum II:

$$I = 1.4333 * 10^{-5} * z^3 - 0.01255 * z^2 + 3.6593 * z - 353.51$$

$$\partial I / \partial z = 4.2999 * 10^{-5} * z^2 - 0.0251 * z + 3.6593 = 0$$

$$z = 282.674° - 270° = 12.674°$$

$$I = 1.815$$

Average Maximum = 1.881

$$\tan(\gamma) = 0.037 : 1.881 = 0.020$$

$$\gamma = 1.135$$

$$\chi = (16.848° + 15.663°) : 2 = 16.256°$$

using Eqns. 22 and 23:

$$\cos(2\Psi) = \cos(2\gamma) * \cos(2\chi) = 0.843$$

$$\Psi = 16.291°$$

$$\tan(\delta) = \tan(2\gamma) : \sin(2\chi)$$

$$\delta = 4.218°$$

Then the index of refraction and thickness are computed. The procedure has to be changed, since the program using the bi-section method does not work every time. First a program generating the index of refraction and phase shift is written; see Appendix D. The program produces the index of refraction *n* to the corresponding phase shift δ for the given azimuth Ψ, as in Appendix E. The index is found for the phase shift computed above. This procedure is an improvement over [28], since the table generated shows a wide range of data and one does not have to assess the index of film at all. The index found is used in the program in the Appendix C that computes the thickness. The third column of cos(x) is for a verification that the cos(x) is smaller than 1.0 at the same time.

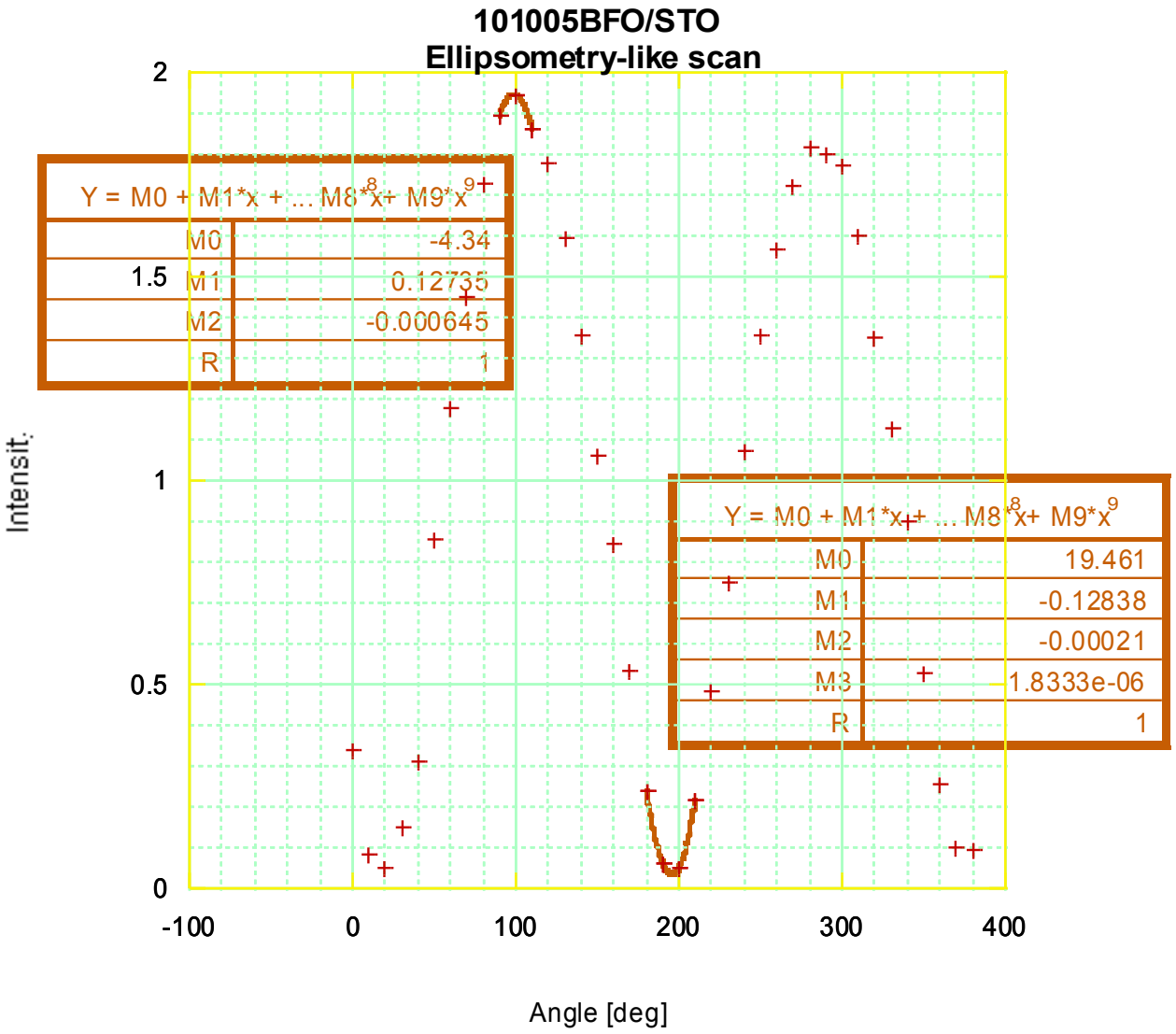

Fig. 27

Ellipsometry-like Scan of 101005BFO/STO with Fit Curves for one maximum and minimum.

The Fresnel scan is performed to verify the scan above and whether the minimum goes to a zero or not. For the most of the scans, the indexes of refraction from the two scans does not correspond. It is probably due to that the sample very inhomogeneous. The Fresnel scan of 101005BFO/STO is in Fig. 27. The minimum that represents the Brewster angle is computed by similar way as for minimum of ellipsometry-like scans.

$$I = 0.018798 * z^2 - 2.7967 * z + 104.24$$

$$\partial I / \partial z = 0.037994 * z - 2.7967 = 0$$

$$z = 74.388°$$

Index of Refraction $n = 3.579$

More complicated and interesting situation appears when the minimum in the Fresnel scan does not go to a zero. Then from ellipsometry-like scan the index of refraction and thickness is computed the data are substituted to RHS of Eqn. 44:

$$r_p * \exp[i * \delta] = r_p' + r_p'' * \exp[-i * x] \qquad (44)$$

where $x = 4 * \pi * \lambda^{-1} * (n + i * k) * d * \cos(\text{asin}(\sin(\theta_i) / n_1))$.

The only unknown is the imaginary part k. Using KaleidaGraph to plot the absolute value of Eqn. 44, one finds the corresponding part *k* for the principal angle obtained from the Fresnel scan.

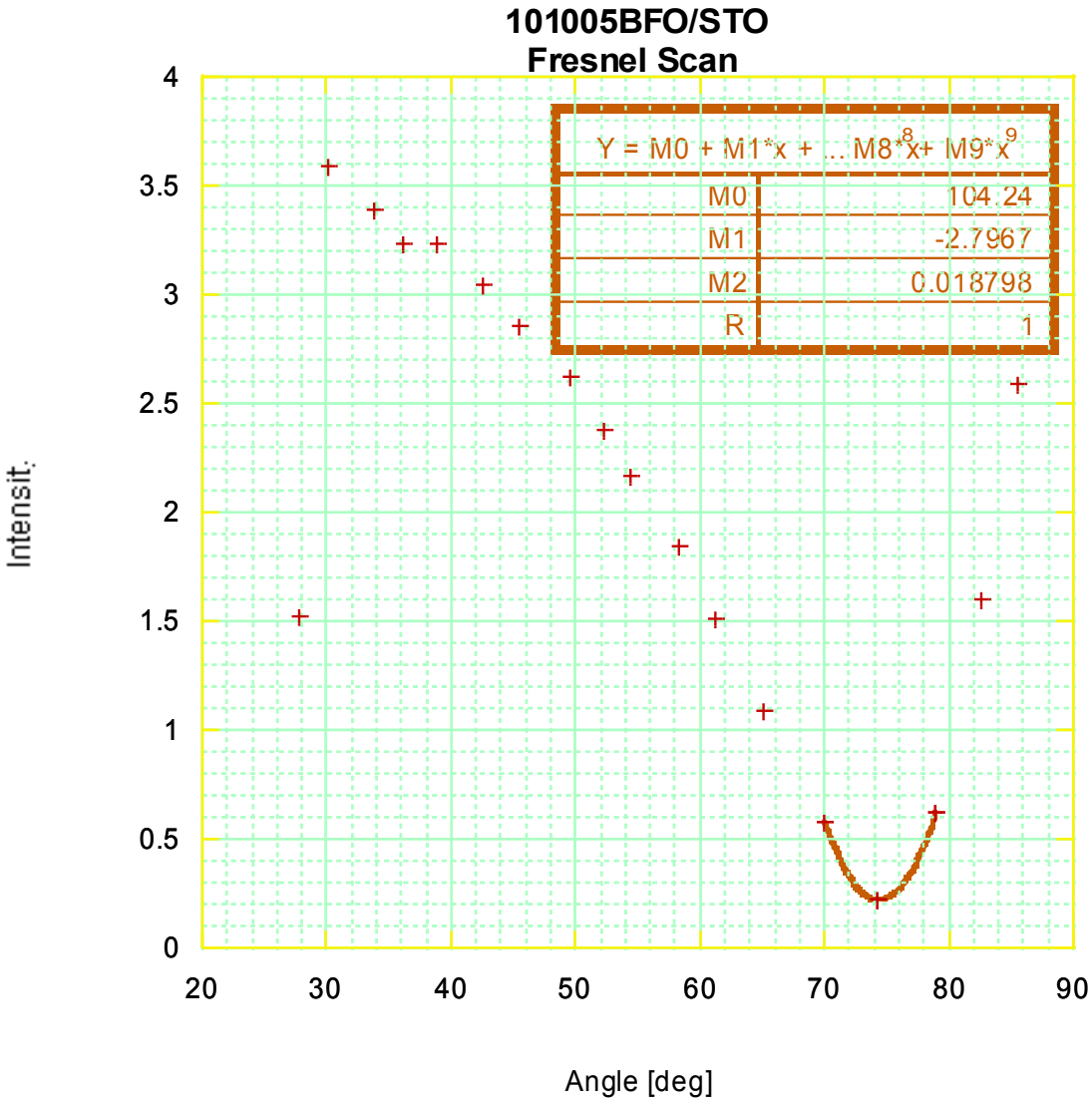

Fig. 28

Fresnel Scan of 101005BFO/STO.

C. Sample Computing of Capacitance vs. Frequency

From the Table V for the sample 021507BFO/STO are taken data that correspond to a sequence of the highest capacitance to the lowest one, and at the same time, and of the lowest conductance to the highest one. It was not always true, mostly either the capacitance or conductance jumped and did not follow the pattern through the range of frequencies; i.e., the conductance is decreased from 17 to 18 kHz in Table V. The set data of the largest difference are put to the Eqn. 39 and using the fact that the ratio of the two sets gets rid of the unknown capacitance the equation is solved for the only unknown contact resistance. This is called the method of ratios.

frequency [kHz]	Capacitance [nF]	Conductance [mS]
10	0.584	0.2429
11	0.577	0.2642
12	0.535	0.2684
13	0.497	0.2720
14	0.463	0.2750
15	0.433	0.2758
16	0.401	0.2771
17	0.374	0.2772
18	0.349	0.2761
19	0.325	0.2735
20	0.307	0.2708

Table V

Measured data of the sample 021507BFO/STO.

In this case, the contact are used the frequencies $2 * \pi * 10$ and $2 * \pi * 20$ rad s^{-1} to compute the contact resistance first:

$$(\omega_2 * C / G) / (\omega_1 * C / G) = \qquad (40)$$

$$= 17 / 10 = [0.142 / (1 – (2.83) * 10^{-4} * r_s)] / [0.149 / (1 – 2.53) * 10^{-4} * r_s)]$$

$$r_s = 3089\ \Omega$$

The capacitance of the film is computing by substitution into Eqn. 35:

$$C_p = 0.374\ nF / [(1 + 0.858)^2 + (0.123)^2] \qquad (41)$$

$$C_p = 1.079 * 10^{-10}\ F$$

Then the relative permittivity *k* of the film is:

$$k = C_p * d / (A * \varepsilon_0) \qquad (42)$$

$$k = 2.438$$

where the area $A = 0.25\ mm^2$

thickness $d = 500$ Å (assessed)

permittivity constant $\varepsilon_0 = 8.854 * 10^{-12}\ F\ m^{-1}$

The relative permittivity *k* is very low and it is due not just of low quality film but as well to the incompatibility of deposited metal and the film. The depositing metal is chromium as a base with the gold on up it. The metal does not stick to the film at all and the needle of the micro-probe scratch the metal off completely.

D. Sample Computing of Capacitance Dependent Current

As well the capacitance as a function of current is measured. For the sample 021507BFO/STO the data and capacitance are substituted into Eqn. 34:

$$C_I = 10*10^{-6}\ A * (7.5 * 10^{-5}\ s - 0\ s) / (4.2333984\ V - 1.6992187\ V)$$

$$C_I = 2.960\ 10^{-10}\ F$$

This is the capacitance of both film and substrate. This measurement is made for the consistency only. If the capacitance is related to Eqn. 43:

$$1 / C_I = 1 / C_f + 1 / C_s \qquad (43)$$

where C_f = capacitance of the film [F cm^{-2}]

C_s = capacitance of the substrate [F cm^{-2}]

The capacitance must be smaller than for the film but it is difficult to compute the capacitance and relative permittivity of the film due to unknown effective area of the substrate. Nevertheless, the capacitance is higher and it is probably due to a mobile charge. When the DC current is applied, more charge is involved as capacitance, while the AC current enforces the mobile charge to move as a current.

E. Hall Effect Measurements

Due to problems with the deposited metal, not having an ammeter to measure pA, and not having sufficiently strong magnetic field, it is not possible to get any data to evaluate mobility, resistivity, and leakage current of the films.

VIII. RESULTS

A. X-ray and RBS Results

The crystallographic and film thickness results from this work are summarized in Table VI. The BFO samples are characterized by relationship between its stoichiometry and epitaxy. If the film keeps stoichiometry of the deposited metals with a ratio even, then the film is epitaxial i.e. 092705BFO/STO. When the ratio is not even, then the film is either twinning or not epitaxial. But there are exceptions, i.e. 022706BFO/STO is not be able to be scanned by RBS to get a chemical composition but it appears to be epitaxial according to the X-ray scans. Another example is the sample 021706BFO/STO, which is not epitaxial but its stoichiometry is perfect, $BiFeO_3$.

There may be two sets of of additional peaks to the family [001] for BFO films. One set corresponds to the plane distance about 2.8 Å and family [011], the other set, with only one peak, corresponding to the plane distance about 3.2 Å, the lattice parameter of 5.6343 Å and plane (1 1 1) of rhombohedral structure [32] . The second set peak occurs at the samples 022707BFO/STO and 020206BFO/STO only.

As well the lattice parameter is bigger than for bulk, on average 2.6%, and it is a = 4.061 Å, which is in according to [33]. The only exception is 100605BFO/STO with the lattice parameter a = 3.959 Å.

The pattern of BTO sample is different. When it is not possible to make RBS analysis, then it is not epitaxial. The samples with known chemical composition are either epitaxial or twinning.

The BTO films don't have any additional peaks and its average lattice parameter a = 3.898 Å that is about 2.4% less than for the bulk lattice parameter a = 3.990 Å but it is almost identical to the lattice of STO, a = 3.905 Å.

Sample	$A_x B_y O_3$	Epitaxial / phases	Deposition	Growth Rate [Å/min]	lattice [Å]	d_{RBS} [Å]	a / ($2^{0.5}$ * x)	Note, x =[Å]
092705BFO/STO	1.00 : 1.00	epitaxial	alternating	3.264	4.057	544.0		
092805BFO/STO	bad	twinning + phase	N/A		4.065	N/A	1.000	+peak 2.873Å
100605BFO/STO	1.06 : 0.35	twinning + phase	alternating	19.698	3.959	3283.0	0.972	+peak 2.882Å
100705BFO/STO	bad	twinning	co-depositing		4.027	N/A	0.989	+peak 2.878Å
101005BFO/STO	1.00 : 1.00	epitaxial / +phase	co-depositing	3.582	4.065	298.5	0.991	+peak 2.900Å
101105BFO/STO	bad	not epitaxial + phase	alternating	N/A	4.065	N/A		
101405BFO/STO	0.64 : 0.64	epitaxial / + phase	co-depositing	4.644	4.074	331.7	1.003	+peak 2.873Å
101405BFO/STO_B	0.64 : 0.64	not epitaxial	co-depositing	0.995	4.066	66.3	1.004	+peak 2.865Å
102005BFO/STO	bad	not epitaxial	co-depositing	3.166	4.076	N/A		
102405BFO/STO	bad	twinning	co-depositing	3.123	4.065	N/A		
111505BFO/STO	0.40 : 0.64	not epitaxial	co-depositing	11.342	4.058	762.9		
111605BFO/STO	1.00 : 1.00	epitaxial	co-depositing	0.371	4.090	39.8		omega scattered
111905BFO/STO	0.75 : 0.88	twinning	co-depositing	1.670	4.067	132.7		
112405BFO/STO	0.60 : 0.69	twinning	co-depositing	4.082	4.065	290.9		sub omega
120805BFO/STO-Nb	0.64 : 0.64	epitaxial	co-depositing	0.875	4.069	145.9		omega double
121505BFO/STO-Nb	0.49 : 0.64	epitaxial	alternating	0.848	4.064	232.2		
122205BFO/STO	bad	not epitaxial	co-depositing	0.916	4.045	N/A		
122705BFO/STO	0.64 : 0.64	epitaxial	co-depositing	0.708	4.071	212.3		
020206BFO/STO	bad	twinning	alternating	1.395	4.063	N/A	1.004	+peak 2.867Å
020906BFO/STO	0.45 : 0.45	twinning	alternating	1.264	4.065	421.4		
021706BFO/STO	1.00 : 1.00	one phase, not epitaxial	co-depositing	17.839	4.072	4459.7		
022106BFO/STO	1.00 : 1.00	epitaxial	co-depositing	N/A	4.045	2809.3		
022706BFO/STO	bad	epitaxial	co-depositing		4.057	N/A	1.016	+peak 2.824Å
051706BTO/STO	0.56 : 1.00	epitaxial	alternating	1.365	3.898	204.8		
060106BTO/STO	bad	twinning	co-depositing		3.897	N/A		
060806BTO/STO	bad	not epitaxial	co-depositing	3.775	3.899	N/A		
062106BTO/STO	bad	not epitaxial	co-depositing		3.897	N/A		omega 4 peaks
062406BTO/STO_Nb	1.00 : 1.00	epitaxial	N/A		3.891	71.1		
062606BTO/STO_Nb	1.20 : 1.20	twinning	N/A		3.906	51.2		
072506BFO/STO	1.00 : 0.90	twinning	co-depositing		4.074	N/A		
072606BFO/STO	0.60 : 0.60	twinning	co-depositing		4.058	N/A		omega double
072706BFO/STO	0.75 : 0.85	not epitaxial	co-depositing		4.022			omega 3 peaks
072806BFO/STO	0.42 :0.48	twinning	co-depositing		4.068			

Table VI

Samples with parameters related to RBS and X-ray scans.

B. Index of Refraction and Thickness

Optical spectroscopy measurements were performed on all samples physically present without any metal deposition in Table VII. Comparing their properties, one can see that the thickness determined by RBS is always smaller than by the optical method and it two cases, for 062406BTO/STO-Nb and 062606BTO/STO-Nb, the difference is very big. There is no way to explain it, since it was not possible to perform an independent scan. Another interesting fact is that the two samples and 060806BTO/STO has the the index of refraction from the Fresnel scan bigger, even the difference is small, and does not depend on whether the sample is epitaxial or not. It is not true for the BFO films. Most of the samples have lower index of reflection from Fresnel scan when the film is not epitaxial. There is an exception, 032107BFO/STO, that is epitaxial according the X-ray scan but the index of refraction from both scans is lower than expecting. The index from the Fresnel scan is only 1.001. As well I have to mention about the sample and 041405BTO/STO, which has index of refraction from the Fresnel scan smaller than 1.0 and it is probably a similar physical phenomenon as for a prism coupling characterization.

On the other hand, most of the indexes of refraction of BFO is in the agreement with other reports. The lowest indexes $n = 1.804$ for not epitaxial and $n = 1.948$ for epitaxial film are still higher than for the porous film grown by the sol – gel method [13], $n = 1.51$, but lower $n = 2.26$ for $\lambda = 700$ nm grown by sol – gel method as well [34]. The highest values of the index are $n = 3.005$ and 3.162 are even higher than any found in articles, $n = 2.95$ [14]. The remaining data of the indexes are more or less close to the expected value $n = 2.6$ [16] and consistent with other reported values as seen in Table VII.

The sample of the scattered light is in Fig. 29. It shows that the films inhomogeneous and it could explain the difference between the indexes of refraction of two optical scans. The samples with both RBS and optical scan are in Table VIII.

Index of Refraction	Wavelength λ [Å]	Deposition	Reference, note
1.51	630	sol-gel	[13], porous
2.05	700	sol-gel	[34], amorphous
2.10	700	pulsed laser	[35], thin
2.13	630	sol-gel	[36], thin
2.26	700	sol-gel	[34], crystalline
2.31	630	sol-gel	[37], thin
2.60	630	sol-gel	[38], nano-crystalline film at T = 550° C
2.95	630	pulsed laser	[14], thin

Table VII

Comparison of the indexes of refraction and depositions.

Sample	$A_xB_yO_3$ x : y	Epitaxial /phase	Deposition	d_{RBS} [Å]	d_S [Å]	N = n + ik	n_F
011005BFO/STO					597.3	2.546 + i0	1.616
041405BTO/STO	0.17:1.11		alternating	230.0	251.1	2.593 + i0	0.862
090105BFO/STO			co-deposition		666.6	2.955+i0.38	2.979
101005BFO/STO	1.00:1.00	epitaxial/ phase	co-deposition	298.5	537.7	2.826 + i0	3.579
102005BFO/STO	bad	not epitaxial	co-deposition	N / A	593.6	2.534 + i0	1.525
102405BFO/STO	bad	twinning	co-deposition	N / A	585.5	2.484 + i0	1.501
111505BFO/STO_B	0.40:0.64	not epitaxial	co-deposition	762.9	855.5	1.934 + i0	1.462
112105BFO/STO	N / A	twinning	co-deposition	N / A	547.1	2.555 + i0	1.911
120205BFO/STO	N / A	not epitaxial	co-deposition	N / A	663.3	1.804 + i0	1.177
122205BFO/STO	bad	not epitaxial	co-deposition	N / A	534.4	3.005 + i0	1.212
020206BFO/STO	bad	twinning	alternating	N / A	488.2	3.162 + i0	2.992
052206BTO/STO	N / A	N / A	alternating	N / A	N / A	0.943 + i0	1.911
060806BTO/STO	bad	not epitaxial	co-deposition	N / A	660.6	1.197 + i0	1.280
062406BTO/STO-Nb	1.00:1.00	epitaxial	N / A	71.1	547.4	2.240 + i0	2.333
062606BTO/STO-Nb	1.20:1.20	twinning	N / A	51.2	422.9	2.230 + i0	2.325
072506BFO/STO	1.00:0.90	twinning	co-deposition	N / A	561.8	2.194 + i0	2.174
072606BFO/STO	0.60:0.60	twinning	co-deposition	N / A	586	2.793 + i0	2.125
102806BFO/STO	N / A	N / A	N / A	N / A	394.5	2.473 + i0	1.454
110606BFO/STO	N / A	N / A	N / A	N / A	527	2.670 + i0	1.608
012907BFO/STO	N / A	N / A	N / A	N / A	439.9	2.405 + i0	3.020
022707BFO/STO	N / A	N / A	N / A	N / A	496.7	2.576 + i0	2.772
032107BFO/STO	N / A	epitaxial	N / A	N / A	742.2	1.948 + i0	1.001

Table VIII

Comparison of samples with RBS and optical scans.

Fig. 29

Three photos of a sample under a laser beam.

Top – Polarized spectrometer used for the optical scans.

Middle – More detailed part of sample under laser beam. The red light appears as yellow on the surface and only as red on the rim.

Bottom – Negative image of the sample. The light dispersions is clearly seen.

C. Capacitance Measurements

Only two samples, 021507BFO/STO and 013107BTO/STO, are deposited with a metal. Due to incompatibility of the metal and films, the capacitance of both samples is very low as well the relative permittivity. It is reflected by the resistivity contact, too. One can see in the photo (Fig. 30) that the metal is easily scratched off with the needle of micro-probe.

The data of the two samples are summarized in Table IX.

From these results no one can make conclusions of the quality of films due to unsuitable deposited metal contacts but it looks that there is a big amount of free moving charge, since the capacitance of two or more capacitors in series ought to be smaller than of each capacitor.

Sample	013107BTO/STO	021507BFO/STO
C_f	7.943 pF	107.9 pF
C_I	269.0 pF	300.4 pF
r_s	844.9 kΩ	3089 Ω
k_f	0.179	2.438
k_I	6.077	6.853

Table IX

Capacitance, relative permittivity, and contact resistance of 013107BTO/STO and 021507BFO/STO.

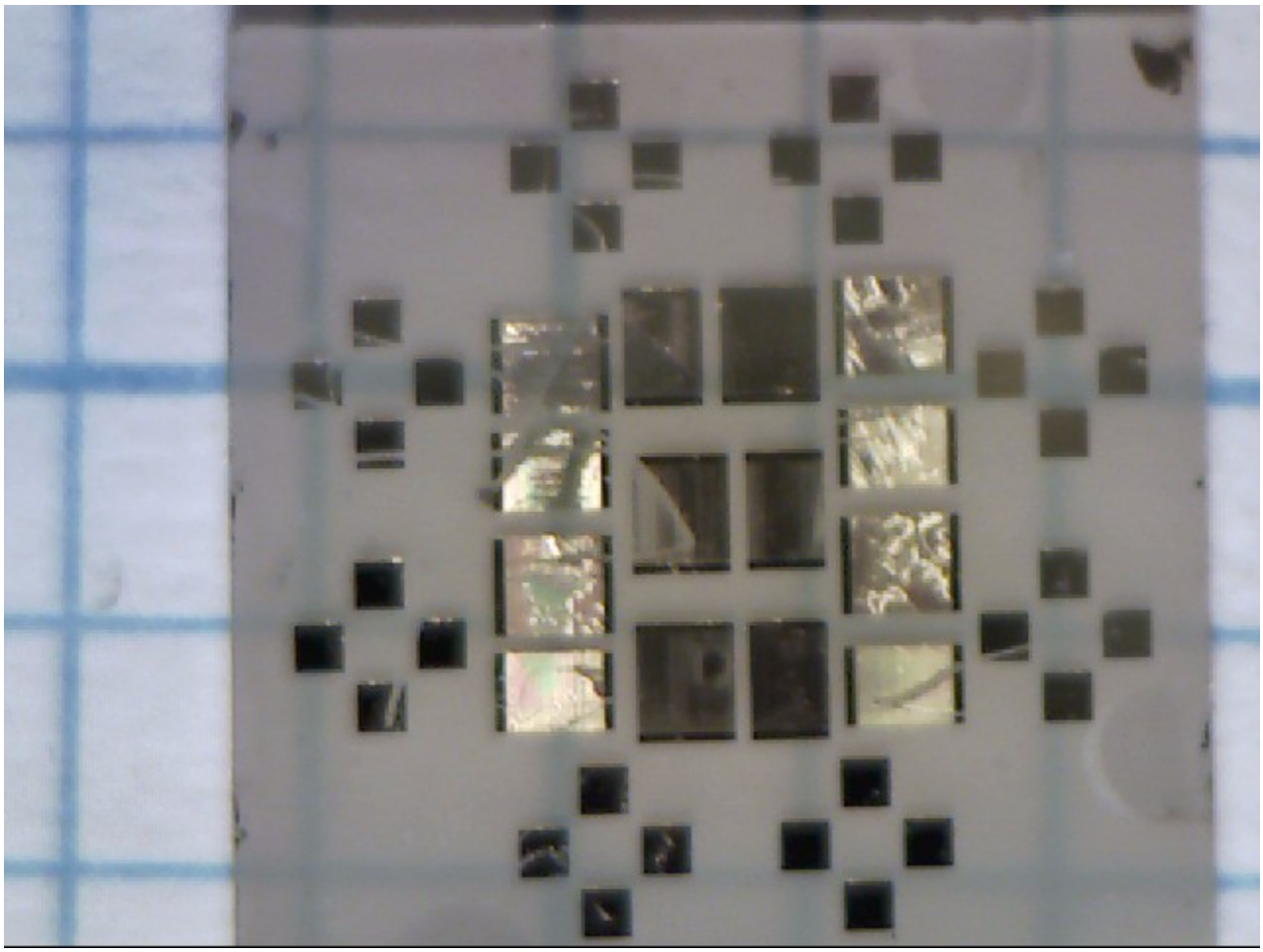

Fig. 30

Photo of 013107BTO/STO after a few runs. The capacitance tests are made on the small squares next to the edge of the sample.

IX. CONCLUSION

The BFO films grow with the average lattice parameter a = 4.061 Å of the family planes [001]. The lattice parameter is bigger than for the bulk BFO by 2.6% but it is consistent with the result for thin films. The indexes of refraction of BFO films are in the range or slightly outside of reported indexes of refraction that are from n = 1.51 to 2.95. The BFO films grown in MBE have the index of refraction from n = 1.934 to 3.162, base on the scans made with the polarizing spectrometer. There were sometimes discrepancies between the index of refraction as measured by the polarizing spectrometer and the Fresnel scan.

The films of BTO are more consistent regarding their properties. It is real that the dissociation energy of BTO plays a role. Their lattice parameters are smaller than for bulk, about 2.4% of the average a = 3.898 Å, but almost identical to the lattice parameter of STO , a = 3.990 Å. The index of refraction is lower than for bulk (N = 2.362 + i1.14) and without any imaginary part. As well the index of refraction is higher for good films (n = 2.240, 2.230) then for a bad one, n = 1.197.

The tests and scans show if the films keep their stoichiometric ratios of metals even, then the film grows epitaxially. The epitaxial film is grown even for a various chemical stoichiometry of $Bi_xFe_xO_3$ and the X-ray diffraction also detects additional peaks of $BiFeO_3$., not just of the family planes {001} indicating that the film is not perfectly monocrystallic. But there are some exceptions and it just shows that to grow BFO is more complicated task than to grow BTO,which has a structure that is more consistent with a composition.

As well the films are inhomogeneous and that it is necessary to design stricter deposition procedures, i.e. to run a deposition of a suitable time to establish a steady conditions, since the first deposition of the week or even day is different from the following ones.

It is both necessary and suitable to involve as many tests as possible and then to determinate which are

preferable to follow and which one not. The tests used as RBS, X-ray, and optical scans show that their properties are related to each other, but on the other hand, only future tests of different kind, i.e. electrical tests, will determine how the tests are complimentary or necessary to fully characterize the materials for the integrated circuit devices.

The tests and examinations above are designed to grow BFO on Si(001).

X. REFERENCES

[1] Darrell G. Schlom, Long-Qing Chen, Xiaoqing Pan, Andreas Schmehl, Mark A. Zurbuchen: "A Thin Film Approach to Engineering Functionality into Oxides", Journal of American Ceramic Society, 2008, V. 91, No. 8, pp. 2429 – 2454

[2] W. Wang, A. V. Virkar: "A conductimetric humidity sensor based on proton conducting perovskite oxides", Sensor and Actuators, B 98 (2004), pp. 282 - 290

[3] N. A. Spalding, M. Fiebeg: "The Renaissance of Magnetoelectric Multiferoics", Science, 2005, V. 309, No. 5733, pp. 391 – 392

[4] W.J. Kim, S.S. Kin, T.K. Song, S.E. Moon, E.K. Kim, S.J. Lee, S.K. Han, M.H. Kwak, H.Y. Kim, Y.T. Kim, H.C. Ryu, C.S. Kim, K.Y. Kang: "Coplanar Waveguide Using Ferroelectric Thin Oxide Film: Dielectric Constant", Journal of Electroceramics, 2004, V. 13, pp. 245 -249

[5] Fernardo Rinaldi: "Basics of Molecular Beam Epitaxy (MBE)", Annual Report 2002, Optoelectronics Department, University of Ulm

[6] http://mxp.physics.unm.edu/s07/Projects/S07_Graphene/intro.html

[7] http://wsi.tum.de/Research/AmannggroupE26/AreasofResearch/Epitaxy

[8] C. Blauuw, F. van der Woude: "Magnetic and Structural Properties of $BiFeO_3$", Journal of Physics C, Solid State Physics, V. 6, 1973, pp. 1422 – 1431

[9] K. Y. Yun, M. Noda, M. Okuyama, H. Saeki, H. Tabata, K. Sat: "Structural and multaferroic properties of $BiFeO_3$ thin films at room temperature", Journal of Applied Physics, V. 96, No. 6, 2004, pp. 3399 – 3403

[10] J. Wang, H. Zheng, Z.Ma, S. Prasertchoung, M. Wutting, R. Droopad, J. Yu, K. Eisenbeiser, R. Ramesh: "Epitaxial $BiFeO_3$ thin films on Si", Applied Physics Letters, V. 85, No. 13, 2004, pp. 2574 – 2576

[11] S. U. Lee, S. S. Kim, H. K. Jo, M. H. Park, J. W. Kim, A. S. Bhalla: "Electrical properties of Cr-doped $BiFeO_3$ thin films fabricated on the p-type Si(100) substrate by chemical solution deposition", Journal of Applied Physics, V. 102, 2007, pp. 104 107-1 - 104 107-5

[12] Z. Quan, W. Liu, H. Su, S. Xu, B. Sebo, G. Fang, M. Li, X. Zhao: "Microstructure, electrical, and magnetic properties of Cr-doped $BiFeO_3$ thin films", Journal of Applied Physics, V. 104, 2008, pp. 084 106-1 - 084 106-10

[13] V. Fruth, R. Ramer, M. Popa, J. M. Calderon-Moreno, E. M. Anghel, M. Gartner, M. Zaharescu, M. Anasastasescu: "Deposition and characterization of $BiFeO_3$ thin films on different substrates", Journal of Material Science, No. 18, 2007, pp. S187 - S190

[14] Amit Kumar, Ram C. Rai, Nicolas J. Podraza, Sava Denev, Mariola Ramirez, Ying-Hao Chu, Lane W. Martin, Jon Ihlefeld, T. Heeg, J. Schubert, Darell G. Schlom, J. Orenstein, R. Ramesh, Robert W. Collins, Janice L. Musfeldt, Venkatraman Gopalan: "Linear and nonlinear optical properties of $BiFeO_3$", Applied Physics Letters, V. 92, 2008, pp. 121915-1 - 121915-3

[15] S. Ohta, T. Nomura, H. Ohta, M. Hirano, H. Hosono, K. Koumoto: "Large thermoelectric performance of heavily Nb-doped $SrTiO_3$ epitaxial film at high temperature", Journal of Applied Physics, V. 97, 2005, pp. 034 106-1 – 034106-4

[16] J.-P. Rivera, H. Schmid: "On birefringence of magnetoelectric $BiFeO_3$", Ferroelectrics, 1997, V. 204, pp. 23 – 33

[17] N. N. Krainik, N. P. Khuchua, V. V. Zhdanova, V. A. Evseev: "Phase Transitions in $BiFeO_3$", Soviet Physics – Solid State, 1966, V. 8, No. 3, pp. 654 – 658

[18] Fernardo Agulló-Lopez, José Manuel Cabrera, Fernando Agulló-Rueda: "Electrooptics - phenomena, materials, and applications", Academic Press, 1994, p. 134

[19] Lifeng Liu, Haizhong Guo, Huibin Lü, Shouyu Dai, Bolin Cheng, Zhenghao Chena: "Effects of donor concentration on the electrical properties of Nb-doped $BaTiO_3$ thin films", Journal of Applied Physics, 2005, V. 97, pp. 054102-1 - 054102-5

[20] Edward D. Palik, edited by: "Handbook of Optical Constants of Solids II", Academic Press, Inc., 1991, p. 798

[21] Francis S. Galaso: "Structure, Properties and Preparation of perovskite-type compounds", Pergamon Press, 1969, pp. 143

[22] http://www.matweb.com

[23] Arthur Linz, Jr.: "Some Electrical Properties of Strontium Titanate", Physical Review, Letters to Editor, V. 91, No. 3, pp. 753 – 754

[24] Edward D. Palik, edited by: "Handbook of Optical Constants of Solids II", Academic Press, Inc., 1991, pp. 1043

[25] L. Hilt Tisingera, R. Liu, J. KulikX. Zhang, J. Ramdani, A. A. Demkov: "Ultraviolet-Raman studies of $SrTiO_3$ ultrathin films on Si", Journal of Vacuum Science Technology B 21.1., Jan - Feb 2003, pp. 53 – 56

[26] Sverre M. Selbach, Mari-Ann Einarsrud, Tor Grande: "On the Thermodynamic Stability of $BiFeO_3$", Chemistry of Materials, 2009, V. 21, No. 1, pp. 169 – 173

[27] Wikipedia: Rutherford Backscattering Spectrometry, http://en.wikipedia.org

[28] Antonín Vasíček: "Polarimetric Methods for the Determination of the Refractive Index and the Thickness of Thin Films on Glass", Journal of Optical Society of America, 1947, V. 37, No. 3, pp. 145 – 153

[29] http://www.eeel.nist.gov/812/effe.htm

[30] http://www.lectroy.com/tm/libraty/LABs/lab418/defaults.asp

[31] D. K. Schroder: "Semiconductor Material and Device Characterization", John Wiley & sons, Inc., 1998, pp. 88 – 90

[32] F. Kubel, H. Schmid: "Structure of Ferroelectric and Ferroelastic Monodomain Crystal of the Perovskite $BiFeO_3$", Acta Cryst., 1990, V. B46, pp. 698 – 702

[33] Khwi Young, Yun, Minoru Noda, Masanori Okuyama, Hiromasa Saeki, Hitoshi Tabata, Keisuke Saito: "Structural and multiferroic properties of $BiFeO_3$ thin films at room temperature", Journal of Applied Physics, 2004, V. 96, No. 6, pp. 3399 - 2403

[34] H. B. Sharma, S. Bobby Singh, Ng Boinis Singh: "Stuctural and optical properties of low temperature synthesized nanostructured $BiFeO_3$ thin films", Physica B, 2011, V. 406, pp. 351 - 353

[35] N. Kumar, A. Kaushal, C. Bhardwaj, D. Kaur: "Effect of La doping on structural, optical and magnetic properties of $BiFeO_3$ thin films deposited by pulsed laser deposition technique", Optoelectronics and Advanced Materials, V. 4, No. 10, 2010, pp. 1497 - 1502

[36] V. W. Li, J. Q. Xue, J. L. Sun, X. J. Meng, Z. M. Huang, J. H. Chu, L. H. Ding, W. F. Zhang "Infrared optical properties of $BiFeO_3$ thin films prepared by chemical solution deposition",

Applied Physics A, V. 87, 2007, pp. 125 – 128

[37] D. J. Huang, H. M. Deng, F. Che, H. Deng, P. X. Yang, J. H. Chu: "Optical properties of $BiFeO_3$ and $Bi_{0.9}La_{0.1}FeO_3$ films on silicon substrates", Journal of Physics: Conference Series 276 (2011) 012168, pp. 1 - 5

[38] Yu Xu, Mingrong Shen: "Structure and optical properties of nanocrystalline $BiFeO_3$ films prepared by chemical solution deposition", Materials Letters, V 62, 2008, pp. 3600 – 3602

APPENDIX A

Attaching a Sample to Its Carrier:

A little bit stretch the holding spring (the spring is almost O shaped).

Put the front mask its front face down.

Insert a sample to the square window (held with 4 arms on its bottom).

Lay the disk with its concave (peak) face down (towards the sample).

Attached the spring using a special tweezers.

Gently push the spring down.

Load the sample on the car. You must put it on the more CCW holes!

Loading a Sample:

Mark the position of each wafer (Car #).

Close the Intro valve (C.W., using the lever).

Close the door/gate:

Turn the turbo pump on (Turbo-V 250).

Close the vent valve (C.W.) {leak checked note}.

Close the N_2 valve (C.C.W.).

Wait until P <= 1 m torr.

Switch the Ion gauge on (Intro).

Intro Chamber:

Wait about an hour to start baking, when f = 56 k rpm.

Heating a sample to outgass: T_{max} = 135 °C, ramp = ± 2 °C/min, until pressure is relatively constant at

10^{-8} torr range.

After cooling off with the same ramp, transfer samples to the buffer chamber:

Open the gate between the Intro and Buffer Chambers.

Move the car to the Buffer Chamber.

Close the gate.

Buffer Chamber:

Align a substrate to the heating station.

Set up the substrate temperature: T_{sub}, ramp = ± 2 °C / min via Heated_Station.

Deposition Chamber:

After transferring a sample from the buffer chamber to the deposition one: close the gate.

Set up the substrate temperature: T_{sub}, ramp = ± 2 °C / min via CAR_Heater.

Set up the effusion temperature: T_{eff}, ramp = ± 2 °C / min (tip and bottom), if Ti is using, then turn the cooling machine on and change the current I according its procedure.

After the temperatures are in steady state: switch the oxygen source on and only then the plasma on (follow a procedure).

Program the deposition.

At the end: plasma off, oxygen off, etc.

Unloading a Sample:

Ion gauge off.

Pump off.

Turn N_2 - knob to open (C.W.) but keep P < 3 psi.

Open the vent valve (C.C.W.) {leak checked note}.

Wait until P > 300 m torr and the turbo is quite.

Open (C.C.W.) the Intro valve. It should take at least 3 min., so don't open it too much. The change of pressure might be about 10 torr / s.

Switching the plasma on:

Adjust the oxygen flow control to desired position.

Switch the plasma on (knob = "up").

Turn the oxygen supply on.

Increase the power by 50 W per at least 30 s steps to desired value.

Adjust the green oxygen knob to get the refractive power as low as possible.

Switching the plasma off:

Decrease the power by 50 W per at least 30 s steps to a zero.

Adjust the oxygen flow to zero (directly).

Turn off the oxygen supply (the green knob).

APPENDIX B

```
program thickindex_Vasik ! program computes a thickness and index from "Vasicek"
real pi, incia, substra, phi, index_sub, index_l, index_u, thick, phi_temp, x, filma
real lambda, index1
parameter (pi = 3.141592654)
parameter (incia = 1.221730) ! = 70.00 deg
parameter (index_sub = 1.5687) ! glass
parameter (lambda = 5893.0) ! green light, [A]
print*, "Results for n1 < ns"
phi = 0.507309 ! phi is actually the angle psi = rp / rs, given from computing
!print*, "phi = ", phi
substra = asin(sin(incia) / index_sub)
!print*, "substra = ", substra
index_l = 1.3 ! given, sub or principal
!print*
index_u = 1.4 ! given, sub or principal
phi_temp = phi
do i = 1, 16
index1 = (index_u + index_l) / 2.0
!print*, "phi_temp = ", phi_temp, "index one = ", index1
!print*, "Going to the subroutine"
! print*
call compu (substra, incia, index1, phi_temp, x, filma)
```

```
! print*, "phi_temp = ", phi_temp
if (phi_temp.gt.phi) then
index_u = index1
else
index_l = index1
end if
!print*, "index_u = ", index_u, "index_l = ", index_l, "phi = ", phi, "phi_temp = ", phi_temp
!print*, "index1 = ", index1
end do
thick = lambda * x / (4 * pi *index1 * cos(filma))
print*, "Azimut Psi = ", phi_temp
print*
print*, "Index is ", index1, " Thickness is ", thick, " A"
contains
subroutine compu (substra, incia, index, phi_temp, x, filma)
real incia, index, rp1, rp2, rs1, rs2, filma, substra, f, g, h, fp, gp, hp, a, b, c, psi, x
real alfa1, alfa2, alfa3, alfa4, beta1, beta2, beta3, beta4
real delta, phi_temp, Aa, Ap, Ba, Bp
filma = asin(sin(incia) / index)
! print*, "index = ", index, " filma = ", filma, "rad"
! print*, "substra = ", substra
! print*
rp1 = tan(incia - filma) / tan(incia + filma)
! print*, "rp1 = ", rp1
```

```
rp2 = tan(filma - substra) / tan(filma + substra)
! print*, "rp2 = ", rp2
rs1 = -sin(incia - filma) / sin(incia + filma)
! print*, "rs1 = ", rs1
rs2 = -sin(filma - substra) / sin(filma + substra)
!print*, "rs2 = ", rs2
! print*
f = rp1**2 + rp2**2
! print*, "f = ", f
g = 1 + rp1**2 * rp2**2
! print*, "g = ", g
h = 2.0 * rp1 * rp2
! print*, "h = ", h
fp = rs1**2 + rs2**2
! print*, "fp = ", fp
gp = 1 + rs1**2 * rs2**2
! print*, "gp = ", gp
hp = 2.0 * rs1 * rs2
! print*, "hp = ", hp
! print*
! print*, "(tan(phi))^2 = ", (tan(phi))**2
! print*
a = h * hp * (1 - (tan(phi))**2)
print*, "a = ", a
```

```
b = f * hp + gp * h - (tan(phi))**2 * (fp * h + g * hp)

print*, "b = ", b

c = f * gp - fp * g * (tan(phi))**2

print*, "c = ", c

print*

psi = (-b - (b**2 - 4.0 * a * c)**0.5) / (2 * a)

! psi is a number, not related to the angle - psi

print*

print*, "mantisa = ", (b**2 - 4.0 * a * c)**0.5 / (2 * a)

print*, "-b / (2 * a ) = ", -b / (2 * a)

print*, "psi = cos(x) =", psi

x = acos(psi)

print*, "x = acos(x) =", x

print*

alfa1 = rp1 + rp2 * cos(x)

!print*, "alfa1 = ", alfa1

alfa2 = 1 + rp1 * rp2 * cos(x)

!print*, "alfa2 = ", alfa2 ! 101

alfa3 = rs1 + rs2 * cos(x)

!print*, "alfa3 = ", alfa3

alfa4 = 1 + rs1 * rs2 * cos(x)

!print*, "alfa4 = ", alfa4

beta1 = rp2 * sin(x)

!print*, "beta1 = ", beta1
```

```
beta2 = rp1 * rp2 * sin(x)

!print*, "beta2 = ", beta2

beta3 = rs2 * sin(x)

!print*,"beta3 = ", beta3

beta4 = rs1 * rs2 * sin(x)

!print*, "beta4 = ", beta4

! print*

Aa = alfa1 * alfa2 + beta1 * beta2

!print*, "Aa = ", Aa

Ap = alfa3 * alfa4 + beta3 * beta4

!print*, "Ap = ", Ap

Ba = alfa1 * beta2 - alfa2 * beta1

!print*, "Ba = ", Ba

Bp = alfa4 * beta3 - alfa3 * beta4

!print*, "Bp = ", Bp

!print*

delta = atan((Aa * Bp + Ap * Ba) / (Aa * Ap - Ba * Bp))

! print*, "delta = ", delta

phi_temp = atan(A * Bp + Ap * B) / ((alfa2)**2 + (beta2)**2) / ((alfa3)**2 + (beta3)**2) /

>> sin(delta)

!print*, "End of Subroutine"

! print*

end subroutine compu

end program thickindex_Vasik
```

APPENDIX C

```
program DirekFikVasik
! This program with the paremeters below from Vasicek computes the thickness directly
real psi, ksi, rp1, rp2, rs1, rs2, index1, lambda, index_sub, pi, incia, thick, x
parameter (lambda = 5893.0) ! Wavelength of light applied, [Å]
parameter (pi = 3.141592654)
parameter (index_sub = 1.5687) ! Index of susbstrate, glass
parameter (incia = 1.222) ! Angle of incidence = 70.0 deg
parameter (index1 = 1.3632) ! Index of the film gotten from Vasicek
parameter (psi = 0.507) ! psi gotten from Vasicek
filma = asin(sin(incia) / index1)
substra = asin(sin(incia) / index_sub)
rp1 = tan(incia - filma) / tan(incia + filma)
! print*, "rp1 = ", rp1
rp2 = tan(filma - substra) / tan(filma + substra)
! print*, "rp2 = ", rp2
rs1 = -sin(incia - filma) / sin(incia + filma)
! print*, "rs1 = ", rs1
rs2 = -sin(filma - substra) / sin(filma + substra)
! print*, "rs2 = ", rs2
f = rp1**2 + rp2**2
print*, "f = ", f
g = 1 + rp1**2 * rp2**2
```

```
print*, "g = ", g

h = 2.0 * rp1 * rp2

print*, "h = ", h

fp = rs1**2 + rs2**2

print*, "fp = ", fp

gp = 1 + rs1**2 * rs2**2

print*, "gp = ", gp

hp = 2.0 * rs1 * rs2

print*, "hp = ", hp

a = h * hp * (1 - (tan(psi))**2)

print*, "a = ", a

b = f * hp + gp * h - (tan(psi))**2 * (fp * h + g * hp)

print*, "b = ", b

c = f * gp - fp * g * (tan(psi))**2

print*, "c = ", c

print*

ksi = (-b - (b**2 - 4.0 * a * c)**0.5) / (2 * a)

! ksi is a number, not related to the angle-psi

! print*

print*, "mantisa = ", (b**2 - 4.0 * a * c)**0.5 / (2 * a)

print*, "-b / (2 * a ) = ", -b / (2 * a)

print*, "ksi = cos(x) =", ksi

x = acos(ksi)

thick = lambda * x / (4 * pi *index1 * cos(filma))
```

```
print*, "x = acos(x) =", x

print*

print*, "thickness = ", thick, "A"

end program DirekFikVasik
```

APPENDIX D

```
program cosXindex ! program generates a tab of index vs. phase shift

real rp1, rp2, rs1, rs2, f, g, h, fp, gp, hp, alf1, alf2, alf3, alf4

real bet1, bet2, bet3, bet4, A, Ap, B, Bp, delta, lambda, psi, ksi

real substra, incia, index_sub, index_u, index1, filma

parameter (pi = 3.141592654)

parameter (incia = 1.0984) ! = 62.9 deg

parameter (index_sub = 2.387) ! STO

! parameter (index_sub = 3.869) ! Si

parameter (lambda = 6350.000) ! red light, [A]

psi = 0.284332 ! = deg, psi is actually the angle psi = rp / rs, given from computing

! print*, "psi = ", psi

substra = asin(sin(incia) / index_sub)

!print*, "substra = ", substra

index1 = 1.6 ! given, sub or principal

!print*

index_u = 3.9 ! given, sub or principal

open (unit = 8, file = 'IndexDelta')

write(8, *) " Index ", " Delta [deg]", " ", " cosX "

write(8, *)

do while (index1.le.index_u)

print*, "index one = ", index1

! print*, "Going to the subroutine"
```

```
filma = asin( sin(incia) / index1)

substra = asin( sin(incia) / index_sub)

print*, "index = ", index1, " filma = ", filma, "rad"

! print*, "substra = ", substra

! print*

rp1 = tan(incia - filma) / tan(incia + filma)

! print*, "rp1 = ", rp1

rp2 = tan(filma - substra) / tan(filma + substra)

! print*, "rp2 = ", rp2

rs1 = -sin(incia - filma) / sin(incia + filma)

! print*, "rs1 = ", rs1

rs2 = -sin(filma - substra) / sin(filma + substra)

! print*, "rs2 = ", rs2

! print*

f = rp1**2 + rp2**2

! print*, "f = ", f

g = 1 + rp1**2 * rp2**2

! print*, "g = ", g

h = 2.0 * rp1 * rp2

! print*, "h = ", h

fp = rs1**2 + rs2**2

! print*, "fp = ", fp

gp = 1 + rs1**2 * rs2**2

! print*, "gp = ", gp
```

```
hp = 2.0 * rs1 * rs2

! print*, "hp = ", hp

! print*

! print*, "(tan(psi_temp))^2 = ", (tan(psi_temp))**2

! print*

a = h * hp * (1 - (tan(psi))**2)

! print*, "a = ", a

b = f * hp + gp * h - (tan(psi))**2 * (fp * h + g * hp)

! print*, "b = ", b

c = f * gp - fp * g * (tan(psi))**2

! print*, "c = ", c

! print*

ksi = (-b - (b**2 - 4.0 * a * c)**0.5) / (2 * a)

! ksi is a number, not related to the angle-psi

if ( abs(ksi).le.(1.0) ) then

print*

print*, "mantisa = ", (b**2 - 4.0 * a * c)**0.5 / (2 * a)

print*, "-b / (2 * a ) = ", -b / (2 * a)

print*

print*, "ksi = cos(x) =", ksi

print*

print*, "index = ", index1

endif

if ( abs(ksi).le.(1.0) ) then
```

```
x = acos(ksi)
!print*, "x = acos(x) =", x
!print*, "b = ", b
!print*, "psi = ", psi
!print*
alf1 = rp1 + rp2 * cos(x)
!print*, "alfa1 = ", alfa1
G:\Plato90\cosXindex.f95
alf2 = 1 + rp1 * rp2 * cos(x)
!print*, "alfa2 = ", alfa2 ! 101
alf3 = rs1 + rs2 * cos(x)
!print*, "alfa3 = ", alfa3
alf4 = 1 + rs1 * rs2 * cos(x)
!print*, "alfa4 = ", alfa4
bet1 = rp2 * sin(x)
!print*, "beta1 = ", beta1
bet2 = rp1 * rp2 * sin(x)
!print*, "beta2 = ", beta2
bet3 = rs2 * sin(x)
!print*,"beta3 = ", beta3
bet4 = rs1 * rs2 * sin(x)
!print*, "beta4 = ", beta4
! print*
A = alf1 * alf2 + bet1 * bet2
```

```
!print*, "Aa = ", Aa

Ap = alf3 * alf4 + bet3 * bet4

!print*, "Ap = ", Ap

B = alf1 * bet2 - alf2 * bet1

!print*, "Ba = ", Ba

Bp = alf4 * bet3 - alf3 * bet4

!print*, "Bp = ", Bp

!print*

delta = atan((A * Bp + Ap * B) / (A * Ap - B * Bp))

!print*, "delta = ", delta

else

x = 0.0

delta = 0.0

endif

write( 8, 20) index1, delta, ksi

20 format (1x, sp, f7.3, " ", sp, e12.3," ", sp, f7.3)

index1 = index1 + 0.001

end do

close (8)

end program cosXindex
```

APPENDIX E

Index	Delta [deg]	cosX
+2.819	+0.000E+00	-1.027
+2.820	+0.000E+00	-1.020
+2.821	+0.000E+00	-1.012
+2.822	+0.000E+00	-1.006
+2.823	+0.139E-01	-0.999
+2.824	+0.336E-01	-0.992
+2.825	+0.454E-01	-0.985
+2.826	+0.547E-01	-0.978
+2.827	+0.626E-01	-0.971
+2.828	+0.696E-01	-0.964
+2.829	+0.759E-01	-0.958
+2.830	+0.817E-01	-0.951
+2.831	+0.872E-01	-0.944
+2.832	+0.923E-01	-0.938
+2.833	+0.971E-01	-0.931
+2.834	+0.102E+00	-0.925
+2.835	+0.106E+00	-0.918
+2.836	+0.110E+00	-0.912
+2.837	+0.114E+00	-0.905
+2.838	+0.118E+00	-0.899

VITA

NAME:	Jiri Vojtech Kabelac
EDUCATION:	B.S., Engineering Physics. University of Illinois at Chicago, Illinois, 1999
	M.S., Material Engineering, University of Vermont, Burlington, Vermont, 2002
	Ph.D., Material Engineering, University of Illinois at Chicago, Illinois, 2011
TEACHING EXPERIENCE	Department of Physics, University of Vermont, Burlington, Vermont: Physics Labs, 1999 - 2002 Department of Civil and Material Engineering, University of Illinois at Chicago, Illinois: Introduction to Materials, Statics, Environmental Engineering, 2003 - 2005 and 2008 – 2010
RESEARCH EXPERIENCE	Department of Electrical Engineering, University of Vermont, Burlington: growing and characterization of Yttria Stabilized Zirconia, 2001 Department of Electrical Engineering, University of Illinois at Chicago, Illinois: Research Assistant, depositing and characterization of perovskites, 2005 – 2008
HONORS	Golden Key, the National Honor Society